CANCER

Systematic single amino acid affinity tuning of CD229 CAR T cells retains efficacy against multiple myeloma and eliminates on-target off-tumor toxicity

Erica R. Vander Mause[1,2,3], Jillian M. Baker[1], Kenneth A. Dietze[1], Sabarinath V. Radhakrishnan[2,4], Thierry Iraguha[5], Destiny Omili[5], Patricia Davis[6,7], Sadie L. Chidester[8], Katarzyna Modzelewska[8], Jens Panse[9], James E. Marvin[5], Michael L. Olson[7], Mary Steinbach[2], David P. Ng[7], Carol S. Lim[3], Djordje Atanackovic[1,2,10], Tim Luetkens[1,2,10]*

T cells expressing chimeric antigen receptors (CARs) have shown remarkable therapeutic activity against different types of cancer. However, the wider use of CAR T cells has been hindered by the potential for life-threatening toxicities due to on-target off-tumor killing of cells expressing low amounts of the target antigen. CD229, a signaling lymphocyte-activation molecule (SLAM) family member, has previously been identified as a target for CAR T cell–mediated treatment of multiple myeloma (MM) due to its high expression on the surfaces of MM cells. CD229 CAR T cells have shown effective clearance of MM cells in vitro and in vivo. However, healthy lymphocytes also express CD229, albeit at lower amounts than MM cells, causing their unintended targeting by CD229 CAR T cells. To increase the selectivity of CD229 CAR T cells for MM cells, we used a single amino acid substitution approach of the CAR binding domain to reduce CAR affinity. To identify CARs with increased selectivity, we screened variant binding domains using solid-phase binding assays and biolayer interferometry and determined the cytotoxic activity of variant CAR T cells against MM cells and healthy lymphocytes. We identified a CD229 CAR binding domain with micromolar affinity that, when combined with overexpression of c-Jun, confers antitumor activity comparable to parental CD229 CAR T cells but lacks the parental cells' cytotoxic activity toward healthy lymphocytes in vitro and in vivo. The results represent a promising strategy to improve the efficacy and safety of CAR T cell therapy that requires clinical validation.

INTRODUCTION

T cells expressing chimeric antigen receptors (CARs) using single-chain variable fragments (scFvs) to target cancer-associated surface antigens are highly effective against several hematologic malignancies, including B cell lymphoma (1) and multiple myeloma (MM) (2, 3). However, their extraordinary cytotoxic activity poses new challenges, such as the unintended killing of healthy cells expressing the targeted antigen, despite often substantially lower amounts (4). In the case of the widely used CD19 CAR T cells, this on-target off-tumor toxicity results in the elimination of healthy B cells (5, 6). Various other CAR T cell approaches have resulted in life-threatening toxicities and even patient deaths due to the targeting of healthy tissues (7–9). It has been shown previously that CAR T cells exert potent antitumor activity across a wide range of affinities (10–12), and many CAR T cell strategies currently in clinical use likely exceed the required affinity threshold. Consequently, low-affinity scFvs have been developed and incorporated into CAR T cell constructs for several cancer targets to increase cancer selectivity as well as CAR T cell persistence and function (13–16). Prior low-affinity scFvs were generated de novo, meaning that these binding domains were not derived from existing and extensively tested high-affinity scFvs already in clinical use. Because of this approach, the new low-affinity scFvs had to, again, undergo rigorous preclinical evaluation with the risk for substantial liabilities, such as off-target reactivity and complex epitopes.

Here, we developed a new affinity-tuning approach for the generation of low-affinity scFv variants derived from existing high-affinity scFvs. We used this approach to generate low-affinity variants of the recently developed CD229 CAR T cells, a potential new treatment for patients with MM. CD229 is a signaling lymphocyte-activation molecule (SLAM) family member with low expression on healthy lymphocytes but high expression on MM cells (17–20). High-affinity CD229 CAR T cells show antitumor activity but suffer from the same on-target off-tumor toxicities as other high-affinity CAR T cells (19). In this study, we demonstrate that CD229 CAR T cells based on systematically optimized low-affinity scFvs show increased selectivity for tumor cells, increased expansion, and maintained antitumor activity in vitro and in vivo. In addition, low-affinity CD229 CAR T cells showed reduced trogocytosis, the transfer of target antigen from tumor cells to CAR T cells (21, 22), potentially augmenting their persistence in vivo.

[1]Department of Microbiology and Immunology, University of Maryland School of Medicine, Baltimore, MD, USA. [2]Hematology and Hematologic Malignancies, Huntsman Cancer Institute, University of Utah, Salt Lake City, UT, USA. [3]Department of Pharmaceutics & Pharmaceutical Chemistry, University of Utah, Salt Lake City, UT, USA. [4]Division of Hematology and Oncology, Medical College of Wisconsin, Milwaukee, WI, USA. [5]Huntsman Cancer Institute, University of Utah, Salt Lake City, UT, USA. [6]Division of Experimental and Clinical Pathology, ARUP Laboratories, Salt Lake City, UT, USA. [7]Department of Pathology, University of Utah, Salt Lake City, UT, USA. [8]Preclinical Research Resource, Huntsman Cancer Institute, Salt Lake City, UT, USA. [9]Department of Oncology, Hematology, Hemostaseology, and Stem Cell Transplantation, University Hospital RWTH Aachen, Aachen, Germany. [10]Department of Medicine and Transplant/Cell Therapy Program, University of Maryland School of Medicine and Marlene and Stewart Greenebaum Comprehensive Cancer Center, Baltimore, MD, USA.
*Corresponding author: Email: tluetkens@som.umaryland.edu

Vander Mause et al., Sci. Transl. Med. 15, eadd7900 (2023)   19 July 2023

1 of 16

RESULTS

Generation of CD229 scFv variants to increase CAR T cell selectivity

CAR T cells targeting the SLAM receptor CD229, based on the fully human scFv 2D3, were previously developed for the treatment of patients with MM (*19*). Although CD229 CAR T cells show efficient targeting of MM cells (Fig. 1A and fig. S1), they also target healthy lymphocytes, including T cells (Fig. 1B), indicating the potential for toxicities. To determine whether the 2D3 CAR construct is a

candidate for affinity tuning to enhance selective killing of MM cells and spare healthy CD229-positive cells, we analyzed the expression of CD229 on MM cells and normal T cells from patients (*N* = 6) with relapsed or refractory MM using flow cytometry. We found that T cells have significantly lower expression of CD229 than MM cells (*P* = 0.0004; Fig. 1C), which indicated that the engineering of a low-affinity CD229 scFv capable of preferentially targeting high-expressing CD229-positive MM cells could potentially reduce off-tumor toxicities (Fig. 1D).
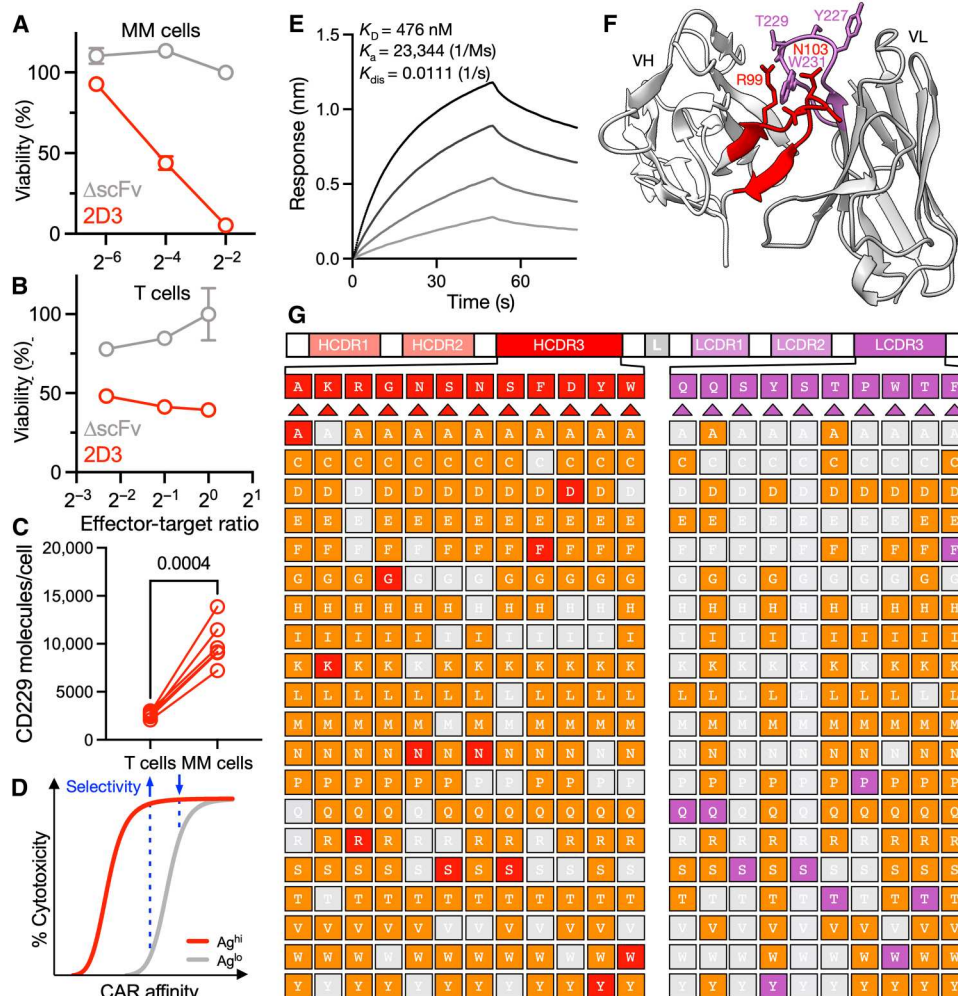

Fig. 1. Generation of 2D3-based CDR3 variant library for the generation of low-affinity CD229 antibodies with increased selectivity. (**A**) Killing of CD229-positive MM cell line U266B1 expressing luciferase by CD229 CAR T cells (2D3) or T cells expressing a CAR without a binding domain (ΔscFv) as determined by luminescence assay. Data indicate means ± SD from technical replicates (*n* = 3). (**B**) Killing of human T cells from a healthy human donor by autologous CD229 CAR T cells (2D3) or T cells expressing a CAR without a binding domain (ΔscFv) as determined by flow cytometry cytotoxicity assay. Data indicate means ± SD from technical replicates (*n* = 3). (**C**) Surface expression of CD229 on MM and T cells from patients with relapsed or refractory MM (*n* = 6). Expression was quantified using Quantibrite beads (BD) after staining of cells with an anti-CD229 antibody (clone HLy9.1.25) and acquisition on a CytoFLEX LX flow cytometer (Beckman Coulter). Statistical significance of differences between cell types was determined by paired two-tailed Student's *t* test, and *P* value is shown. (**D**) Theoretical curve of relationship between CAR affinity and targeting of cells with high antigen expression (Ag^hi) and low antigen expression (Ag^lo). Arrows and dotted lines indicate the relative amount of selectivity at different CAR affinities. (**E**) Sensorgram of 2D3 binding to CD229. Equilibrium (K_D) and rate constants (on-rate, K_a; off-rate, K_{dis}) of the 2D3 scFv were determined by biolayer interferometry (BLI). Biotinylated 2D3 was immobilized on a SA biosensor, and the recombinant extracellular domain of CD229 was added in the following concentrations: 2, 1, 0.5, and 0.25 μM. Sensorgram indicates binding curves for descending CD229 concentrations. Plot shows a representative result of three independent experiments. (**F**) Structure of the 2D3 scFv as predicted by AlphaFold2 (pLDDT scores in table S1), with the GS linker omitted. CDR3 loops of the variable heavy (red) and the variable light (purple) chains as well as exposed residues are highlighted. (**G**) Schema of single amino acid substitution 2D3 CDR3 variant library indicating residues represented in library (orange). Missing variants (gray) and wild-type residues (red, heavy chain residues; purple, light chain residues) are highlighted.
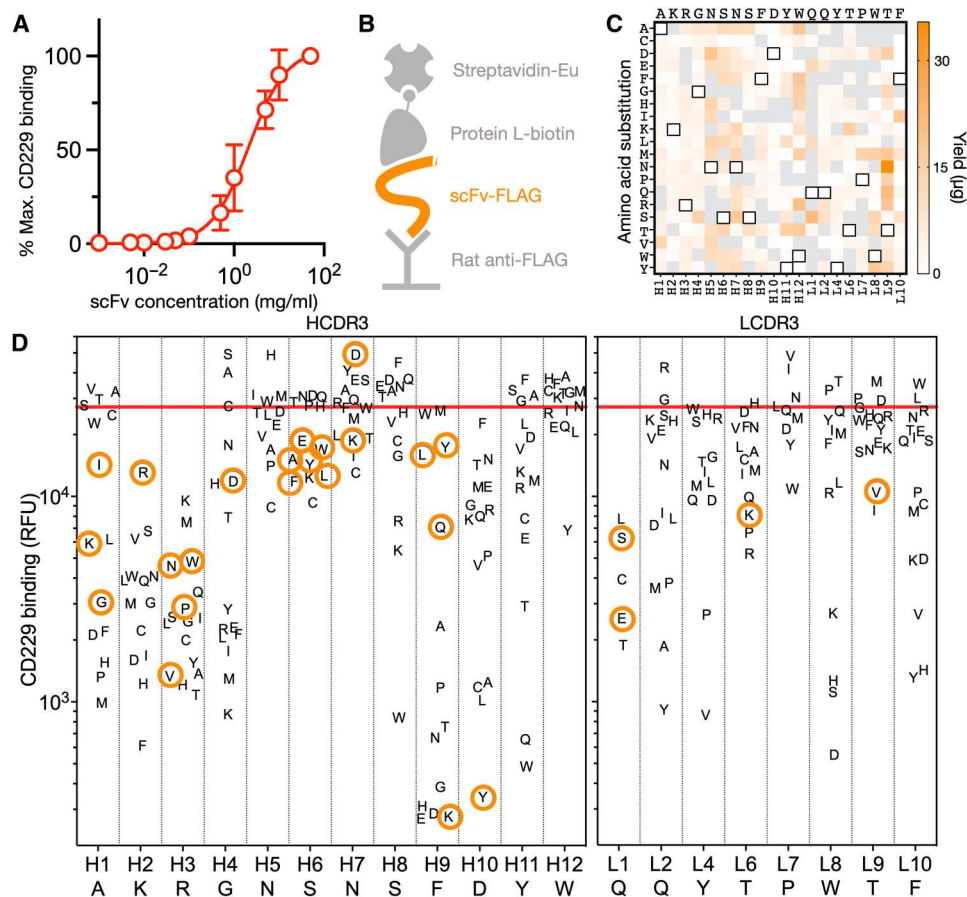
Fig. 2. Single amino acid substitutions result in reduced CD229 binding. (**A**) Concentration dependence of 2D3 scFv binding to recombinant CD229 as determined by solid-phase TRF assay. Data indicate means ± SD from technical replicates (n = 3). (**B**) Schema of solid-phase assay for the determination of FLAG-tagged scFv (orange) concentrations using rat IgG2a λ anti-FLAG antibody, biotinylated protein L, and SA-europium (Eu). (**C**) Total yield of 2D3 scFv variants from autoinduction cultures as determined by assay illustrated in (B). White squares with black outlines indicate amino acids in wild-type 2D3. Gray squares indicate lack of measurable expression of the respective clone. Plot shows representative result of two independent experiments. (**D**) Binding of all expressed 2D3 heavy (H) and light (L) chain CDR3s (HCDR3 and LCD3, respectively) variants at 2 ng/μl to recombinant CD229 as determined by solid-phase TRF assay. Red line indicates wild-type 2D3 binding to CD229. Orange circles indicate variants selected for downstream assays on the basis of amino acid position and binding signal. Plot shows representative result of two independent experiments. RFU, relative fluorescence units.

Affinity tuning of CAR binding domains has previously been shown to reduce targeting of cells with low expression of the targeted antigen (*11*). Compared with other commonly used CAR binding domains, such as the CD19-specific scFv FMC63 (*23*), we found that the affinity of 2D3 is already relatively low at 476 nM (Fig. 1E). Considering the high specificity and preclinical characterization of 2D3, as well as the established antitumor activity and functionality of 2D3-based CAR T cells (*19*), we developed an affinity-tuning approach to generate low-affinity scFv variants of 2D3. Our derivative affinity-tuning approach was carried out by comprehensively mutating the complementarity-determining region 3 (CDR3) of both heavy and light chains of the parental 2D3 scFv (Fig. 1F). Mutagenesis was followed by high-throughput screening of variant scFvs and comprehensive characterization of variant CAR T cells. We generated 305 single amino acid substitution variants of 2D3 (Fig. 1G), with the goal of reducing 2D3 affinity without altering the CD229 epitope, 2D3 specificity, CAR T cell expansion, and antitumor activity.

Single amino acid substitutions result in reduced CD229 binding

Identification of antibodies with reduced affinity represents a relatively uncommon objective in antibody discovery and poses unique challenges when developing appropriate screening approaches. Most common primary antibody screening assays, such as standard solid-phase binding assays using large sets of nonpurified antibodies, are unable to differentiate between expression and affinity. As expected, this was also the case for 2D3, which showed a clear dependence of CD229 binding on antibody concentration, especially in concentration ranges commonly observed in standard high-throughput expression cultures (Fig. 2A). When screening for high-affinity antibodies, this may be acceptable because the highest assay signals are likely the result of a combination of high affinity and high expression, both being desirable properties. In the case of low-affinity antibody screening, however, the potential conflation of low-expressing/high-affinity antibodies with high-expressing/low-affinity antibodies would render such data relatively meaningless. We, therefore, developed a high-throughput scFv
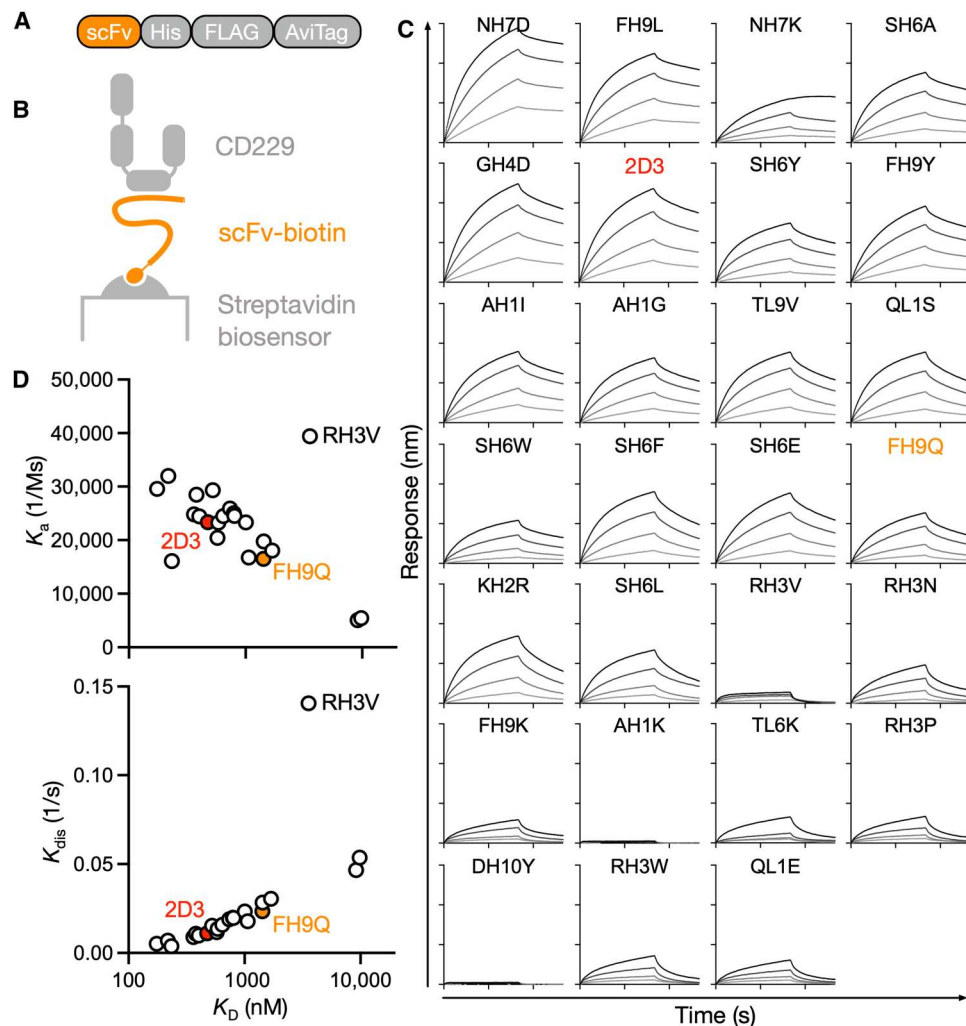
Fig. 3. Affinity-tuning approach results in predominantly off-rate–driven affinity reductions. (**A**) Schema of construct used for production of biotinylated 2D3 scFv variants (orange) including C-terminal AviTag to facilitate in vivo biotinylation. (**B**) Schema of BLI setup used for kinetic characterization of CD229 binding. Biotinylated 2D3 variants (orange) were immobilized on streptavidin biosensors, and the recombinant extracellular domain of CD229 was added in the following concentrations: 2, 1, 0.5, and 0.25 μM. (**C**) Sensorgrams of 2D3 (red), variant FH9Q (orange), and other variants were determined using Octet K2 (Sartorius). Plots show representative result of two independent experiments. (**D**) Correlation between on-rate and off-rate (K_a and K_{dis}) and equilibrium (K_D) constants of 2D3 (red), variant FH9Q (orange), and other variant scFvs as determined by BLI.

quantification assay relying on the binding of protein L to the κ light chain in 2D3 (Fig. 2B) and determined total scFv yields of all generated variants using a time-resolved fluorescence (TRF) assay (Fig. 2C). As expected, substitutions to cysteine and proline generally resulted in poor antibody expression, whereas alanine and threonine substitutions appeared to be tolerated well in various positions (Fig. 2C). In addition, we found that some positions were able to accommodate almost any amino acid. This included some unexpected positions, such as asparagine in position H5, an exposed residue in the center of the groove formed by both CDR3 loops, as well as tryptophan in H12 and threonine in L9 (Fig. 2C). Several substitutions appeared to improve expression, consistent with established approaches to improve antibody solubility through mutation of noncontact residues (24, 25). After normalization of antibody concentrations, we next determined binding to recombinant CD229 in a standard solid-phase binding assay

(Fig. 2D). Although most mutations did not reduce 2D3 variant binding to CD229, and some, as expected, increased binding, the comprehensive mutagenesis approach taken allowed the identification of a large set of scFvs showing various amounts of reduction in binding. Alanine scanning is one of the most widely used techniques to reduce protein-protein binding (26), but our results show that, in many positions, alanine substitutions did not alter binding, whereas nonalanine substitutions did. In addition, alanine substitutions never represented the variants with the lowest binding signal in any position.

Together, our data indicate that comprehensive single amino acid substitution may be preferable to conventional mutagenesis strategies and is able to generate large sets of antibodies showing reduced antigen binding even in already relatively low-affinity binders. On the basis of scFv expression and CD229 binding data, we then selected 26 2D3 scFv variants for downstream analyses.

Table 1. Single amino acid substitution results in a broad range of affinities. Equilibrium (K_D), on-rate (K_a), and off-rate (K_{dis}) constants of 2D3 variants were determined using an Octet K2 BLI instrument (Sartorius). Data are representative of two independent experiments.

Clone	K_D (nM)	K_a (1/M·s)	K_{dis} (1/s)
NH7D	175	29,590	0.0052
FH9L	218	32,007	0.0070
NH7K	234	16,084	0.0038
SH6A	380	28,502	0.0108
GH4D	402	24,421	0.0098
2D3	476	23,344	0.0111
SH6Y	524	29,323	0.0154
FH9Y	575	20,420	0.0117
AH1I	585	23,268	0.0136
AH1G	644	24,487	0.0158
TL9V	736	25,885	0.0190
QL1S	791	25,039	0.0198
SH6W	803	24,513	0.0197
SH6F	1,006	23,307	0.0234
SH6E	1,065	16,737	0.0178
FH9Q	1,425	16,507	0.0235
KH2R	1,431	19,747	0.0283
SH6L	1,689	18,046	0.0305
RH3V	3,565	39,427	0.1406
RH3N	9,157	5,088	0.0466
FH9K	9,835	5,452	0.0536
AH1K	>10,000	50,315	0.9477
TL6K	>10,000	1,337	0.0635
RH3P	>10,000	755	0.0679
DH10Y	>10,000	8,164	0.8991
RH3W	>10,000	595	0.0703
QL1E	>10,000	558	0.0688

Affinity-tuning approach results in predominantly off-rate–driven affinity reduction

To confirm that single amino acid substitution mutagenesis resulted in relevantly altered affinities and rate constants, we next purified (fig. S2) in vivo biotinylated 2D3 variant scFvs (Fig. 3A). We then subjected these scFvs to biolayer interferometry (BLI) using streptavidin (SA) biosensors and recombinant CD229 (Fig. 3B), allowing the use of relatively high analyte concentrations, needed for the characterization of low-affinity binders (27). This process facilitated the characterization of very weak binders (Fig. 3C). Affinities of 2D3 variants with single amino acid substitutions ranged from 175 to >10,000 nM (Table 1), and we observed a close correlation between antibody affinity (K_D) and TRF binding (fig. S3). Differences in affinity were generally driven by changes in scFv off-rate, the rate of dissociation of binders from CD229 (Table 1). This result is likely related to the use of a solid-phase binding assay for primary variant screening, which may have biased clone selection toward variants with faster off-rates. In contrast to this finding, we observed a reduction in the on-rate of variants in which arginine in H3 was replaced (Fig. 3C and Table 1). An exception to this finding is RH3V, which showed a faster on-rate but also a much faster off-rate (Fig. 3D). These data suggest a key role of the H3 arginine in the orchestration of the 2D3 paratope and, among other possibilities, might point to a model of 2D3 binding to CD229 in which RH3 binding facilitates interactions by other residues. Single amino acid substitution together with BLI resulted in the identification of a set of clones with a wide range of mostly off-rate–driven differences in affinity and provided initial data regarding the mode of 2D3-CD229 binding, which may aid future optimization.

CD229 CAR T cells based on variant scFvs can be manufactured, show efficient CAR surface expression, and allow identification of clones with increased selectivity

Optimal CAR affinity remains an active area of research but likely depends on various parameters, such as need for selectivity, epitope, as well as antigen and CAR density. Ideally, CAR affinity for a given target antigen will be chosen empirically, thus requiring a sufficiently large set of binders with different affinities available for CAR construction. We therefore converted all 26 selected low-affinity CD229 scFvs into CAR constructs containing 4-1BB and CD3ζ signaling domains (Fig. 4A) and produced primary human CAR T cells using a standard manufacturing process (Fig. 4B). It has previously been shown that even parental 2D3-based CAR T cells can be manufactured without the CAR T cells targeting each other because CD229 is down-regulated upon anti-CD3/anti-CD28 bead activation early during manufacturing (19). We determined the viability and total CAR T cell yields on day 7 of manufacturing and found that yields varied substantially between constructs (Fig. 4C), possibly indicating increased tonic signaling in some variants (28, 29). Considering the differences in soluble scFv expression between variants (Fig. 2C), we next determined CAR surface expression of wild-type 2D3 and all variant CAR constructs, as well as T cells expressing a CAR without a binding domain (ΔscFv). Although all variant constructs expressed similar amounts of the linked green fluorescent protein (GFP) reporter, two constructs, FH10K and AH1K, showed relatively low CAR surface expression, and two other constructs, DH10Y and RH3N, did not show any CAR surface expression at all (Fig. 4D). One construct, TL9V, showed a bimodal distribution, potentially indicating recombination during retroviral packaging. We next determined whether mutagenesis had resulted in altered antitumor activity by determining killing of MM cells by all variant CAR T cells at multiple effector-target ratios. In the absence of CAR surface expression normalization, we found that several constructs showed reduced tumor cell killing. This reduced cytotoxicity is likely due to the substantially reduced affinity of those variants. Several constructs, including SH6A, GH4D, FH9Y, AH1I, AH1G, and FH9Q, showed antitumor activity comparable to 2D3 (Fig. 4E). Next, we set out to determine whether reducing CAR affinity resulted in increased selectivity by measuring killing of purified T cells (fig. S4). At an effector-target ratio of 0.5:1, we found that numerous constructs with reduced cytotoxic activity against tumor cells also showed reduced killing of T cells (Fig. 4F). However, among the variants showing comparable or increased tumor cell killing, several constructs showed reduced T cell killing in this screening assay, indicating increased selectivity for
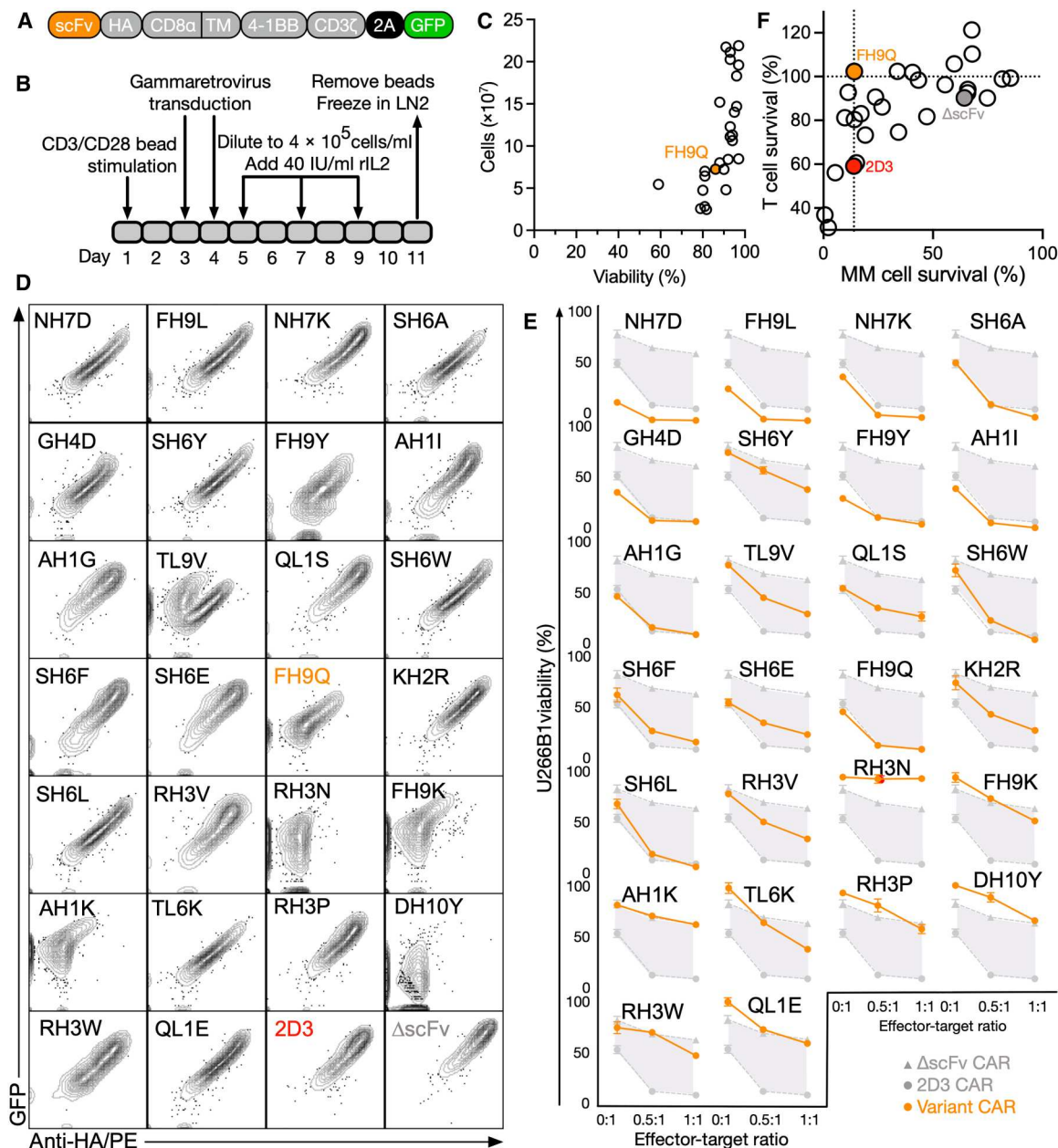
Vander Mause *et al.*, *Sci. Transl. Med.* **15**, eadd7900 (2023) 19 July 2023

5 of 16

Fig. 4. Multiple HCDR3 variants maintain antitumor activity but exhibit minimal T cell killing. (**A**) Schema of variant scfv- (orange) and 4-1BB–based second-generation CAR construct with green fluorescent protein (GFP) reporter (green). (**B**) Schema of the gammaretrovirus-based CAR T cell production process. T cells were isolated from healthy human donor PBMCs using CD3/CD28 activation beads (day 1), transduced with concentrated gammaretroviral particles (days 3 and 4), and expanded in the presence of interleukin-2 (IL-2) before freezing (day 11). (**C**) Correlation between CAR T cell yield and viability of 26 2D3 variant CARs. 2D3 variant FH9Q is highlighted in orange. (**D**) Surface expression of 2D3 (red), variant FH9Q (orange), and other variant CARs as determined by anti-hemagglutinin (HA) tag staining and GFP reporter expression using flow cytometry. (**E**) Cytotoxic activity of ΔscFv (gray triangle), 2D3 (gray circle), and variant CAR T cells (orange) against MM cell line U266B1 expressing luciferase at indicated effector-target ratios using a luminescence-based cytotoxicity assay. Data indicate means ± SD from technical replicates (n = 3). (**F**) Correlation of cytotoxic activity of 2D3 variant CAR T cells against MM cells and T cells after 16 hours of coculture at an effector-target ratio of 0.5:1. Data indicate mean percentage of remaining target cells from technical replicates (n = 3). Dotted lines indicate percentages of killing of U266B1 cells by 2D3 CAR T cells (vertical) and untreated T cells (horizontal). FH9Q (orange) CAR was selected for downstream assays on the basis of increased selectivity and antitumor activity (orange). Parental 2D3 CAR T cells are highlighted in red.
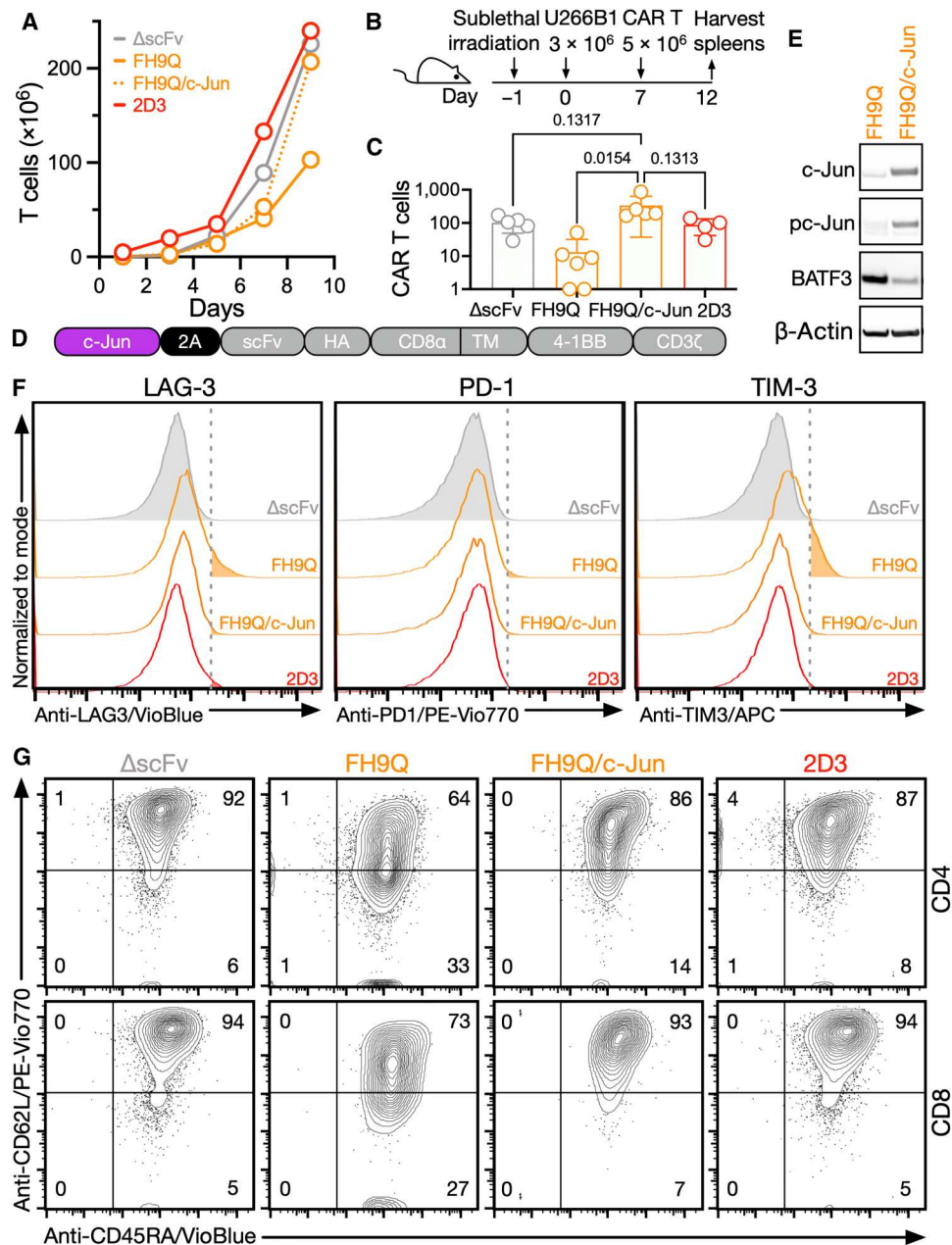
Fig. 5. Overexpression of c-Jun increases expansion of low-affinity CD229 CAR T cells and promotes a stem-like phenotype. (**A**) Expansion of CD229 CAR T cells during manufacturing as determined by cell counting. Data are representative of three independent experiments. (**B**) Schema of in vivo experiment to determine CAR T cell expansion. Sublethally irradiated NSG mice were injected on day 0 with 3×10^6 U266B1 cells by tail vein. Seven days after tumor cell inoculation, animals were injected by tail vein with 5×10^6 ΔscFv, 2D3, or FH9Q CAR T cells with or without overexpression of c-Jun. (**C**) Mice were euthanized on day 12, and CAR T cell numbers were determined by flow cytometry. Data indicate means ± SD from four to six animals per group and are representative of two independent experiments. Statistical differences between conditions were determined by two-sided Student's *t* test, and *P* values are shown. (**D**) Retroviral construct used for the simultaneous expression of CARs and c-Jun (purple). A self-cleaving 2A sequence was included to facilitate separate GFP reporter expression. (**E**) CAR T cells on day 9 of production were lysed and analyzed by Western blot using primary antibodies against the indicated proteins. β-Actin was used as a loading control. CAR T cells on day 12 of production were analyzed by flow cytometry for (**F**) surface expression of exhaustion markers and (**G**) T cell phenotype. Data are representative of two independent experiments.

Fig. 6. Low-affinity CD229 CAR T cells demonstrate preferential killing of target cells with high CD229 expression, resulting in the sparing of normal T cells. Killing of luciferase-expressing (**A**) parental CD229neg K562 cells and K562 cells engineered to express different amounts of CD229 and (**B**) MM cell lines natively expressing different amounts of CD229. Numbers above the plots indicate average number of CD229 molecules on the surfaces of the respective target cells as determined by flow cytometric bead quantification. Target cell killing was determined by luciferase-based cytotoxicity assay. Data indicate means ± SD from technical replicates (*n* = 3). (**C**) Killing of U266B1 cells expressing luciferase by HAint-sorted CD229 CAR T cells after a 16-hour coculture as determined by luciferase-based cytotoxicity assay. Data indicate means ± SD from technical replicates (*n* = 2). (**D**) Killing of T cells from a healthy donor by autologous HAint-sorted CD229 CAR T cells in a 16-hour in vitro coculture at an effector-target ratio of 1:1. Data indicate means ± SD from technical replicates (*n* = 3), and *P* values are shown. Statistical differences between conditions were determined by two-sided Student's *t* test. (**E**) Quantification of CD229 molecules on bulk lymphocyte subsets from four healthy donors as determined by flow cytometry. Data indicate means ± SD from technical replicates (*N* = 3), and *P* values are shown. Statistical differences between cell types were determined by two-sided Student's *t* test. (**F**) Killing of naïve (CD19+CD27−) and memory (CD19+CD27+) B cells from a healthy donor by autologous CD229

CAR T cells in a 6-hour in vitro coculture at an effector-target ratio of 1:1. Data indicate means ± SD from technical replicates (*n* = 3). Statistical differences between conditions were determined by one-way ANOVA followed by Tukey's post hoc test, and *P* values are shown. (**G**) Viability of healthy autologous T cell subsets after 6 hours of coculture with the indicated CAR T cells at an effector-target ratio of 2:1 as determined by flow cytometry. Data indicate means ± SD from technical replicates (*N* = 3). Statistical differences between conditions were determined by two-way ANOVA followed by Tukey's post hoc test, and *P* values are shown. (**H**) Schema of short-term in vivo experiment using non–tumor-bearing NSG mice to determine targeting of healthy T cells by CD229 CAR T cells. Mice were injected with 5 × 10^6 PBMCs and, 2 days later, with autologous CAR T cells by tail vein. Animals were euthanized on day 5, and spleens were harvested for flow cytometry analysis. (**I**) Numbers of CD3pos HA/CARneg healthy human T cells as determined by flow cytometry per 50,000 events in spleens from mice injected with CD229 CAR T cells. Data indicate means ± SD from three to five animals, and *P* values are shown. Statistical differences between conditions were determined by two-sided Student's *t* test. (**J**) Sixteen hours of cytotoxicity assay to determine relative targeting of MM and healthy T cells by CD229 CAR T cells using flow cytometry. T cells (5 × 10^4) and U266B1 cells (5 × 10^4) were cocultured with 1 × 10^5 CD229 CAR T cells, and relative killing was determined by flow cytometry. Numbers indicate total cell numbers within the respective gates normalized using counting beads. (**K**) Surface expression of CD229 on healthy T cells after coculture with indicated CAR T cells for 8 hours at an effector-target ratio of 5:1 as determined by flow cytometry.
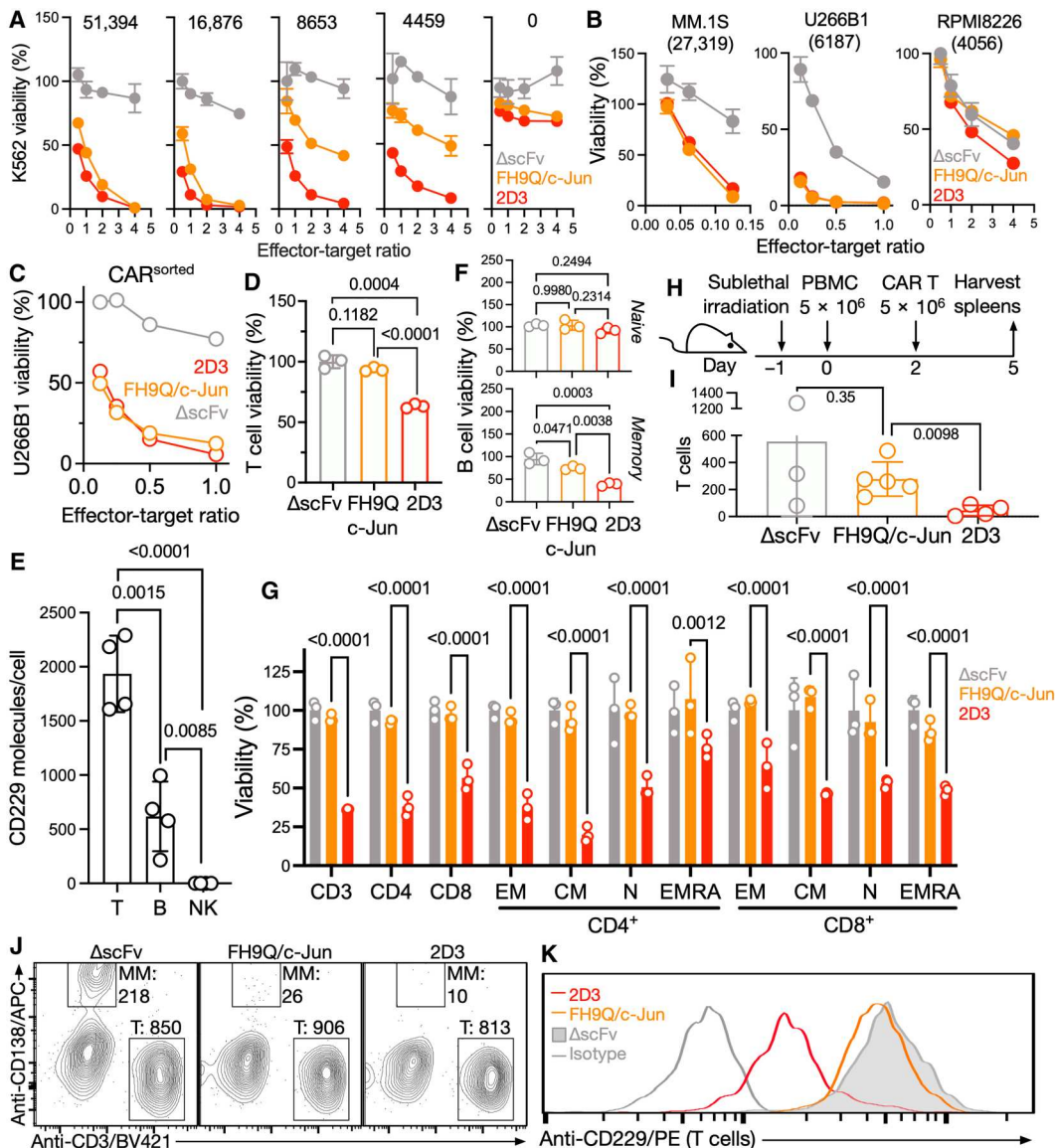
Vander Mause *et al.*, *Sci. Transl. Med.* **15**, eadd7900 (2023)   19 July 2023

8 of 16

tumor cells. For downstream analyses, we selected one construct, FH9Q, which appeared to show minimal killing of T cells, maintained antitumor activity (Fig. 4F), and showed acceptable amounts of cell expansion (Fig. 4C) and CAR expression (Fig. 4D).

Overexpression of c-Jun promotes low-affinity CD229 CAR T cell expansion and stem-like phenotype

FH9Q CAR T cells, like many of the other variants (Fig. 4C), showed reduced expansion compared with ΔscFv CAR T cells during in vitro production (Fig. 5A). In addition, we observed reduced expansion of FH9Q CAR T cells in a short-term in vivo experiment using MM tumor-bearing NOD.Cg-$Prkdc^{scid}$ $Il2rg^{tm1Wjl}$/SzJ (NSG) mice injected with CAR T cells (Fig. 5, B and C). This is in direct contrast to the parental 2D3-based CAR T cells, which expanded comparably to ΔscFv CAR T cells (Fig. 5A) (19). In principle, reduced expansion could be a sign of CAR T cell fratricide. However, we had previously observed that T cells down-regulate CD229 upon activation with anti-CD3/anti-CD28 beads (19) and found that CD229 expression was similarly reduced in ΔscFv, 2D3, and FH9Q CAR T cells during production (fig. S5), indicating that fratricide is unlikely to be the cause of reduced FH9Q CAR T cell expansion.

We next considered the possibility of reduced FH9Q CAR T cell expansion due to tonic signaling. We hypothesized that FH9Q may be prone to aggregation because we had observed reduced surface expression compared with 2D3 (Fig. 4D), and it had previously been shown that membrane-bound scFvs with higher amounts of aggregation exhibit reduced surface expression (30). Aggregation of CARs, mediated by the CAR binding domain, had in turn been shown to result in reduced in vitro and in vivo expansion due to increased tonic signaling (28)—spontaneous T cell activation by the CAR in the absence of antigen (28). As a result, the persistent signaling leads to the rapid depletion of c-Jun, a component of the T cell–activating AP-1 transcription factor (29). Overexpression of c-Jun was shown to efficiently rescue function and expansion of CAR T cells evidencing tonic signaling (29). We therefore generated an FH9Q CAR construct to simultaneously overexpress c-Jun (Fig. 5D), which resulted in increased c-Jun expression (Fig. 5E and fig. S6, A and B). Overexpression of c-Jun restored FH9Q CAR T cell expansion in vitro (Fig. 5A) and in vivo (Fig. 5C). c-Jun overexpression was associated with reduced expression of the inhibitory transcription factor basic leucine zipper ATF-like transcription factor 3 (BATF3) (Fig. 5E). In addition, c-Jun expression resulted in reduced expression of the coinhibitory/exhaustion markers lymphocyte activation gene 3 (LAG-3) and T cell immunoglobulin and mucin-domain containing 3 (TIM-3; Fig. 5F), which are associated with reduced CAR T cell function (31). Furthermore, c-Jun overexpression reduced the number of terminally effector differentiated FH9Q CAR T cells at the end of production (Fig. 5G), a population associated with poor long-term CAR T cell persistence (32). In addition, c-Jun overexpression increased the proportion of CD95+ T memory stem cells (Fig. 5G and fig. S7), which are associated with increased in vivo expansion and persistence (33). These results demonstrate that c-Jun overexpression can efficiently mitigate deleterious effects of tonic signaling resulting from CDR-directed mutagenesis of existing CAR binding domains. For the following in vitro and in vivo analyses, we used c-Jun–overexpressing FH9Q CAR T cells (FH9Q/c-Jun).

FH9Q/c-Jun CAR T cells preferentially target cells with high expression of CD229 because of their low affinity, resulting in the sparing of healthy lymphocytes

We observed preferential killing of MM cells compared with healthy T cells by FH9Q CAR T cells in our cytotoxicity screening assay (Fig. 4F). We next asked the question whether this ability to discriminate between target cells is due to a difference in CD229 expression. We therefore engineered parental CD229neg K562 cells to express CD229 using lentiviral gene transfer and subsequently generated populations of K562 cells expressing different amounts of CD229 by repeated cell sorting. We then cocultured the sorted K562 target cells with low-affinity FH9Q/c-Jun CAR T cells, high-affinity 2D3 CAR T cells, and ΔscFv CAR T cells. We found that 2D3 CAR T cells were able to kill K562 cells expressing any amount of CD229 and only spared CD229neg K562 cells (Fig. 6A). In contrast, FH9Q/c-Jun CAR T cells showed comparable killing of target cells expressing at least 16,876 copies of CD229 but showed limited cytotoxic activity below this antigen density. This indicated that the reduction in affinity allows FH9Q/c-Jun CAR T cells to discriminate between CD229high and CD229low cells. To corroborate this finding, we analyzed the ability of FH9Q CAR T cells to target a set of MM cell lines endogenously expressing different amounts of CD229. We found that, similar to high-affinity 2D3 CAR T cells, FH9Q/c-Jun CAR T cells killed the CD229high cell line MM.1S as well as the CD229int cell line U266B1 (Fig. 6B). In contrast, we found that the CD229low MM cell line RPMI-8226 did not respond to treatment with FH9Q/c-Jun CAR T cells and only showed minimal killing by 2D3 CAR T cells. The density of CD229 molecules on the surfaces of RPMI-8226 cells is lower than the CD229 density on primary human MM cells (Fig. 1C), and we therefore hypothesized that FH9Q/c-Jun CAR T cells would still be able to efficiently target primary human MM cells. We found that, in cytotoxicity assays using primary MM cells, FH9Q/c-Jun CAR T cells eliminated primary tumor cells in four of four samples obtained from patients with MM (fig. S8).

In addition to the difference in affinity, we had observed that FH9Q CAR T cells showed lower CAR surface expression (Fig. 4D). We speculated that this difference in CAR expression between FH9Q and 2D3 CARs could have contributed to the increased selectivity of FH9Q CAR T cells. To determine the influence of CAR surface expression on selectivity, we next sorted 2D3, FH9Q/c-Jun, and ΔscFv CAR T cells to normalize for CAR surface expression (fig. S9). In comparing the ability of sorted and unsorted 2D3 CAR T cells to kill CD229int U266B1 cells, we did not observe reduced killing by sorted 2D3 CAR T cells (fig. S10). We next compared the ability of 2D3 and FH9Q/c-Jun CAR T cells sorted for comparable CAR surface expression to kill MM cells and found that killing by these cells remained identical as well (Fig. 6C). In addition, secretion of major effector cytokines in response to MM target cells was comparable between sorted FH9Q/c-Jun and 2D3 CAR T cells (fig. S11). In a direct coculture of CAR T cells with healthy lymphocytes, we observed significantly reduced killing of healthy T cells by FH9Q/c-Jun CAR T cells compared to 2D3 CAR T cells even after normalization of CAR surface expression (P < 0.0001; Fig. 6D). These data indicate that differences in CAR surface expression at the amounts observed for FH9Q/c-Jun and 2D3 do not contribute to the increased selectivity of FH9Q/c-Jun CAR T cells.
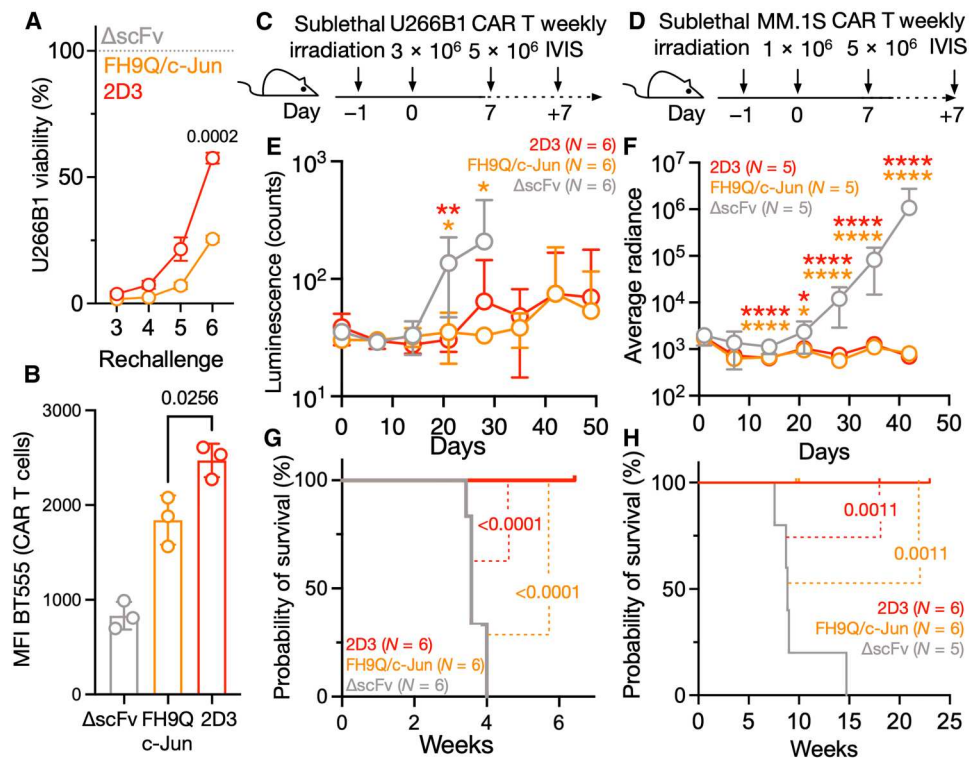
Vander Mause *et al.*, *Sci. Transl. Med.* **15**, eadd7900 (2023)   19 July 2023

9 of 16

Fig. 7. Low-affinity CD229 CAR T cells maintain long-term anti-MM activity in vitro and in vivo. (**A**) Killing of luciferase-expressing U266B1 cells by CD229 CAR T cells in a serial in vitro coculture assay. CAR T cells were rechallenged every 24 hours with MM cells, and luminescence was measured before each rechallenge. Data indicate means ± SD from technical replicates ($n = 3$). The statistical difference between conditions at the last time point was determined by two-sided Student's t test, and P value is shown. (**B**) Membrane transfer from U266B1 cells stained with Biotracker 555 to CD229 CAR T cells after a 4-hour coculture at an effector-target ratio of 4:1 using flow cytometry. Data indicate means ± SD from technical replicates ($n = 3$). Statistical difference between conditions was determined by two-sided Student's t test, and P value is shown. Schemas of in vivo experiments to determine the efficacy of low-affinity CD229 CAR T cells against luciferase-expressing MM cell lines (**C**) U266B1 and (**D**) MM.1S. NSG (U266B1) or NRG (MM.1S) mice were injected intravenously with 3×10^6 U266B1 cells or 1×10^6 MM.1S cells on day 0 and treated with 5×10^6 CD229 CAR T cells on day 7. Bioluminescence of mice intravenously injected with (**E**) U266B1 cells or (**F**) MM.1S cells was determined using an in vivo imaging system (IVIS). Data indicate mean ± SD from five or six animals per group. Statistical significance of differences between ΔscFv and CD229 CAR T cell treatment groups at individual time points was determined by Mann-Whitney U test. Orange (difference between ΔscFv and FH9Q) and red (difference between ΔscFv and 2D3) asterisks indicate significance level (*$P < 0.05$, **$P < 0.01$, and ****$P < 0.0001$). Cumulative survival of (**G**) U266B1 or (**H**) MM.1S tumor–bearing mice treated with CD229 CAR T cells. Statistical significance was determined by log-rank test, and P values are shown. Vertical lines indicate animals censored because of death in the absence of tumor burden as determined by IVIS.

Next, we performed a detailed analysis of the targeting of healthy CD229-expressing cells by FH9Q/c-Jun CAR T cells. CD229 expression has previously been shown to be restricted to lymphocytes in human tissues (*19, 34*). Analyzing the number of CD229 molecules on the surfaces of the major lymphocyte subsets from healthy human donors, we found that T cells express the highest density of CD229 molecules, followed by B cells (Fig. 6E). Natural killer (NK) cells have previously been shown to have very low CD229 expression (*19, 34*), and they remained below the detection limit of our assay. We next analyzed the cytotoxic activity of high- and low-affinity CD229 CAR T cells against these lymphocyte subsets. Using in vitro cocultures, we found that treatment with FH9Q/c-Jun CAR T cells did not affect NK cell viability (fig. S12). We next analyzed the effect of CD229 CAR T cells on healthy B cells. We had previously shown that 2D3-based CAR T cells specifically target memory B cells but spare naïve B cells (*19*). We found that, compared with 2D3 CAR T cells, FH9Q/c-Jun CAR T cells show only minimal targeting of autologous memory B cells from a healthy human donor, and both low- and high-affinity CD229 CAR T cells spare naïve B cells (Fig. 6F). Although we had not

observed targeting of healthy bulk T cells by FH9Q/c-Jun CAR T cells (Fig. 6D), we next performed a more detailed analysis because of their comparably high expression of CD229, which could potentially result in the targeting of individual T cell subsets. We found that 2D3 CAR T cells killed autologous healthy human donor–derived T cells across the various subsets (Fig. 6G), with particularly pronounced targeting of CD4^{+} central memory T cells ($P < 0.0001$). In contrast, FH9Q/c-Jun CAR T cells did not show significant changes in T cell numbers compared with nontargeting ΔscFv CAR T cells across all groups ($P > 0.05$; Fig. 6G). In addition, in a 5-day in vivo cytotoxicity experiment using non–tumor-bearing NSG mice injected with healthy human donor–derived peripheral blood mononuclear cells (PBMCs) and autologous CAR T cells, we did not observe any targeting of healthy T cells by FH9Q/c-Jun CAR T cells in vivo (Fig. 6, H and I). These data indicate that the reduced affinity of FH9Q/c-Jun effectively prevents the targeting of NK cells, B cells, and T cells.

We next asked the question whether targeting of healthy lymphocytes by low- and high-affinity CD229 CAR T cells may be affected by the presence of MM cells. In a mixed target coculture

containing MM cell line U266B1 and healthy autologous T cells as targets, we again observed increased selectivity of FH9Q/c-Jun CAR T cells (Fig. 6J). However, in this assay, T cell killing by 2D3 CAR T cells appeared lower than in the single-target in vitro assay (Fig. 6D) and in vivo (Fig. 6I), suggesting that 2D3 CAR T cells may already provide a degree of selectivity in the presence of tumor cells. Together, in contrast to 2D3 CAR T cells, FH9Q/c-Jun CAR T cells did not show killing of any T cells (Fig. 6, D, G, I, and J) and only minimal killing of B cells (Fig. 6F) from autologous healthy human donors as demonstrated using in vitro coculture assays and a short-term in vivo cytotoxicity experiment.

Previously, we had observed that exposure of healthy T cells to 2D3 CAR T cells results in the selection of a population of CD229^{low} healthy T cells in vitro and in vivo (19). Analyzing CD229 expression on healthy T cells after coculture with 2D3 or FH9Q/c-Jun CAR T cells, we again observed the emergence of a CD229^{low} T cell population when T cells were treated with 2D3 CAR T cells (Fig. 6K). This selection of a CD229^{low} T cell population did not occur when healthy T cells were treated with FH9Q/c-Jun CAR T cells. This result further substantiates the lack of targeting of healthy T cells by FH9Q/c-Jun CAR T cells.

Overall, our data demonstrate that the ability of FH9Q/c-Jun CAR T cells to discriminate between CD229^{high} and CD229^{low} target cells likely results from their reduced affinity and not a difference in CAR surface expression. These low-affinity CD229 CAR T cells efficiently target primary human MM cells and MM cell lines expressing the same amount of CD229 found on primary human MM cells while sparing healthy human donor T cells, B cells, and NK cells.

Low-affinity CD229 CAR T cells are highly effective against MM in vivo

We next asked whether the reduction in CAR affinity would result in incomplete tumor cell killing or suboptimal CAR T cell stimulation leading to reduced long-term disease control by FH9Q/c-Jun CAR T cells. To answer this question, we first performed an in vitro rechallenge assay using the MM cell line U266B1 and observed that FH9Q/c-Jun CAR T cells showed significantly increased long-term tumor cell killing compared with 2D3 CAR T cells ($P = 0.0002$; Fig. 7A). This finding may be related to the overexpression of c-Jun together with FH9Q or more physiological T cell stimulation by low-affinity CAR constructs (13) but could also be the result of reduced trogocytosis, the transfer of target antigen from tumor cells to CAR T cells, by low-affinity CAR T cells. To determine how much trogocytosis is conferred by FH9Q/c-Jun CAR T cells compared with 2D3 CAR T cells, we determined the amount of target antigen and membrane transferred from the MM cell line U266B1 to CAR T cells using flow cytometry. We found that FH9Q/c-Jun CAR T cells had transferred significantly less tumor cell membrane ($P = 0.0256$; Fig. 7B) and target antigen ($P = 0.0017$; fig. S13) than 2D3 CAR T cells, which may have contributed to improved CAR T cell persistence and long-term tumor cell killing in the rechallenge assay.

Next, we performed two in vivo experiments to compare the ability of low-affinity FH9Q/c-Jun CAR T cells to control MM compared with high-affinity 2D3 CAR T cells. NSG or NOD.Cg-Rag1[tm1Mom] Il2rg[tm1Wjl]/SzJ (NRG) mice were injected by tail vein with the indicated numbers of luciferase-expressing human MM cell lines U266B1 (Fig. 7C) and MM.1S (Fig. 7D). One week after

tumor cell injection, 5×10^6 CAR T cells were injected by tail vein, and tumor burden was determined weekly using an in vivo imaging system (IVIS). We found that both 2D3 and FH9Q/c-Jun CAR T cells significantly reduced CD229^{int} U266B1 (Fig. 7E) and CD229^{high} MM.1S tumor burden (Fig. 7F) and prolonged survival compared with ΔscFv CAR T cells ($P = 0.0011$; Fig. 7, G and H). Together, these data indicate that FH9Q/c-Jun CAR T cells exhibit long-term antitumor activity similar to 2D3 CAR T cells against MM tumors with CD229 expression comparable to that observed on primary human MM cells.

DISCUSSION

CAR T cells have revolutionized cancer immunotherapy, but there is a critical need for the development of safer and more effective CAR T cell approaches to achieve more widespread adoption of CAR T cell treatment and increased patient benefit. A key challenge remains on-target off-tumor toxicity, the CAR T cell–mediated killing of healthy cells showing expression of the target antigen, albeit at generally substantially lower amounts. This not only leads to clinically relevant toxicities of existing CAR T cell approaches but also currently prevents the use of otherwise viable target antigens because of their shared expression on healthy tissues. Different combinatorial logic-gate approaches have been developed to address this issue, including AND-gates (35–38) (requiring recognition of multiple antigens) and NOT-gates (39) (requiring recognition of a single antigen in the absence of another) but have not yet been tested in the clinic. An alternative to these strategies is CAR affinity tuning, which has come into focus for its effect on tumor selectivity and CAR T cell function (13–16) and does not require the identification and validation of an appropriate second antigen like in the abovementioned logic-gate approaches. In this study, we describe a new approach for the development of minimally modified low-affinity antibody variants based on established and extensively tested scFvs that does not require detailed structural information including the scFv's exact epitope. Focusing on recently developed CD229 CAR T cells, which, in addition to targeting MM, had shown substantial killing of healthy T and B cells expressing CD229 (19), we demonstrate that the low-affinity variants produced using this approach show increased selectivity and improved CAR T cell function without altering the original epitope and specificity. Most variants generated using our approach show a predominantly off-rate–based reduction in affinity, likely as a consequence of using a solid-phase binding assay for primary variant screening. Data regarding the relative contribution of on-rate and off-rate on CAR T cell signaling remain scarce, but prior approaches to modulate CAR affinity have also predominantly focused on changes in off-rates (40–42). This includes one of the most advanced constructs, a low-affinity CD19 CAR with a predominantly off-rate–driven reduction in affinity, which has already demonstrated clinical benefits of this approach (13, 41).

An important consideration when reducing CAR affinity is the potential effect on the ability of the resulting CAR T cell product to prevent escape of tumor cells with low expression of the targeted antigen. We show here that the CD229^{low} cell line RPMI-8226, with antigen expression substantially lower than that observed in primary patient samples, does not respond to treatment with low-affinity CD229 CAR T cells. Although this is a logical consequence of increasing the antigen density threshold through reduction of

Vander Mause *et al.*, *Sci. Transl. Med.* **15**, eadd7900 (2023)   19 July 2023

11 of 16

CAR affinity, careful consideration of the probability of immune escape through this mechanism is essential. In the case of MM, CD229 has been shown to be highly and homogeneously expressed within individual tumor samples ([17–20], [43]), and CD229 function appears important to maintain the malignant phenotype ([17], [44]). These observations suggest that the emergence of CD229^{low} MM cells may be unlikely, but clinical trials will be necessary to ultimately answer this question.

A key limitation of this study involving the engineering of a low-affinity scFv derived from an existing high-affinity scFv is that our work focused exclusively on the targeting of CD229. Given the unbiased mutagenesis approach we used to generate low-affinity variants, we, however, hypothesize that low-affinity scFvs against different tumor antigens could be generated in the same manner. In addition, we have identified three potential pitfalls to our approach that may limit its generalizability as a robust method for generating low-affinity scFvs. (i) The systematic affinity-tuning approach could introduce tonic signaling in variant CAR T cells despite only minor changes to the binding domain. Overexpression of c-Jun in low-affinity CD229 CAR T cells can overcome this problem by rendering the cells resistant to the downstream effects of tonic signaling. However, it is likely that the success of this solution depends on the degree of tonic signaling. An alternative strategy to address the problem of tonic signaling and to improve CAR T cell function in general is to use protease-sensitive CAR constructs ([45], [46]). In these systems, small molecule–mediated protease inhibition allows tight control over CAR surface expression, preventing early exhaustion resulting from tonic signaling, maintenance of a stem-like phenotype, and increased antitumor activity even when using aggregation-prone CAR constructs. (ii) scFvs with very high affinities may require multiple iterations of mutagenesis to achieve a sufficient reduction in affinity. (iii) For some parental scFvs, it may not be possible to generate variants within the required affinity window depending on their binding mode.

Most cancer treatments aim to strike a balance between efficacy and toxicity. In the case of affinity-tuned CD229 CAR T cells, the challenge was to identify an optimal affinity to maximize targeting of tumor cells to prevent escape of low antigen–expressing tumor cells and to simultaneously reduce the killing of healthy T and B cells. In this study, we showed that systematic, single amino acid mutagenesis of CDR3s was able to produce anti-CD229 scFv variants with a wide range of affinities. In addition, we were able to successfully identify a new low-affinity CAR construct (FH9Q/c-Jun) that eliminated on-target off-tumor effects and retained desirable CAR T cell properties such as expansion, CAR expression, persistence, and, most importantly, antitumor activity. FH9Q/c-Jun CAR T cells are a promising step at striking an optimal balance between efficacy and toxicity of CD229 CAR T cells for the treatment of patients with MM. However, ultimately, only a clinical trial can determine the therapeutic value and the toxicity of low-affinity CD229 CAR T cells.

MATERIALS AND METHODS
Study design
The objective of the study was to reduce the on-target off-tumor toxicity of CD229 CAR T cells by affinity-tuning the CAR's antigen binding domain. We first developed an unbiased approach for the mutagenesis of the CD229 binding domain using single amino acid substitutions, expressed and purified the resulting soluble binding domains, and determined their binding to recombinant CD229. We carried out a functional screening of selected CAR constructs to identify constructs with increased selectivity for MM cells over healthy lymphocytes and selected one construct, FH9Q, which maintained on-target activity against MM cells but decreased targeting of T cells. To limit tonic signaling in FH9Q CAR T cells, we overexpressed the transcription factor c-Jun and showed increased expansion, reduced expression of exhaustion markers, and increased T memory stem cell markers. We validated the increased selectivity of FH9Q/c-Jun CAR T cells with various in vitro cytotoxicity assays using three MM cell lines, four primary MM samples, a tumor cell line engineered to express different amounts of CD229, and primary lymphocyte subsets. In addition, we quantified the antitumor activity of FH9Q/c-Jun CAR T cells in two MM mouse models. Numbers of samples and experimental replicates are indicated in the respective figure legends.

Study approval
The retrospective analysis of patient samples for the expression of CD229 was approved by the Institutional Review Board at the University of Utah (protocol 77285-19). Collection of primary MM samples for cytotoxicity assays was approved by the Institutional Review Board at the Medical College of Wisconsin (protocol PRO00037896) and the ethics committee at the Medical Faculty of RWTH Aachen (EK number 206/09). Animal experiments were approved by the institutional animal care and use committee at University of Maryland Baltimore (protocol 1021001) and the University of Utah (protocol 18-1104).

Cell lines and primary human cells
U266B1, MM.1S, RPMI-8226, K562, and Phoenix-Ampho cells were purchased from the American Type Culture Collection (ATCC) and cultured according to ATCC instructions. Lenti-X 293T cells were purchased from Takara and cultured according to the manufacturer's instructions. Cell lines were authenticated by their respective supplier. Healthy donor buffy coats were obtained from the Blood Centers of America and the New York Blood Center, and PBMCs were isolated from buffy coats by density gradient using FicollPaque (GE) as previously described ([19]).

Flow cytometry expression analysis
Flow cytometry staining and analyses were performed as previously described ([19]). CD229 surface expression was determined using a mouse monoclonal anti-CD229 antibody (clone HLy9.1.25). Other antibodies used for flow cytometry analyses are listed in table S2. Commercially available antibodies were used at dilutions recommended by the respective manufacturer. To determine absolute numbers of CD229 molecules on the surface of cell populations, we generated standard curves using fluorescence quantification beads for allophycocyanin (Bangs Laboratories, catalog no. 823) or phycoerythrin (BD, catalog no. 340495) at the same instrument settings according to the respective manufacturer's instructions. For the analysis of CD229 expression on tumor cells and T cells from patients with MM, data were acquired on CytoFLEX LX (Beckman Coulter) and analyzed using Kaluza 2.1 (BC). To determine killing of healthy T cell subsets by CD229 CAR T cells, data from cocultures were acquired on a full-spectrum Aurora flow cytometer (Cytek). All other flow cytometry data were acquired on an

Vander Mause *et al.*, *Sci. Transl. Med.* **15**, eadd7900 (2023) 19 July 2023

12 of 16

LSR Fortessa or LSR II flow cytometer (BD) and analyzed using FlowJo 10 (BD).

Single amino acid substitution library production

Parental 2D3 was cloned into the pSANG10 bacterial expression plasmid (47), and the single amino acid substitution library produced was generated using high-throughput gene synthesis by Twist Bioscience. Individual mutations were confirmed by Sanger sequencing. To produce single-site biotinylated scFvs, a C-terminal AviTag was added to the pSANG10 expression constructs (pSANG10-Avi), and scFv constructs in the bacterial expression plasmids were transformed into BL21(DE3) cells (Lucigen) containing the pBirAcm plasmid (Avidity).

scFv expression and purification

Monoclonal scFvs were expressed overnight using 96-well deep well blocks or in 25 ml of MagicMedia *Escherichia coli* autoexpression medium (Thermo Fisher Scientific). Periplasmic extracts (PPEs) were generated from autoinduction cultures using standard procedures. For some experiments, scFvs were purified by immobilized metal affinity chromatography using Ni–nitrilotriacetic acid resin (Thermo Fisher Scientific). Concentrations of purified scFvs were determined by bicinchoninic assay (BCA; Thermo Fisher Scientific). pSANG10-Avi clones were expressed in the same way in the presence of 50 μM free D-biotin (Sigma-Aldrich).

Interferon-γ enzyme-linked immunosorbent assay

Supernatants were harvested from 96-well overnight cocultures and immediately frozen at −80°C. Interferon-γ (IFN-γ) concentrations were determined by standard curve using a commercial enzyme-linked immunosorbent assay (ELISA) kit according to the manufacturer's instructions (BioLegend). Absorbance was measured on a multimode plate reader (Tecan).

CAR T cell production

Selected scFvs were cloned into a previously described second-generation 4-1BB–based CAR construct (19) in the gammaretroviral SFG backbone. For some constructs, the full-length sequence of human c-Jun (UniProt, P05412) was synthesized and cloned upstream of the respective CAR separated by a P2A sequence (Twist Bioscience). Amphotropic gammaretrovirus was generated by transfection of Phoenix-Ampho cells (ATCC, catalog no. CRL-3213) using the SFG-based transfer plasmids using Lipofectamine 2000 according to the manufacturer's instructions. Virus-containing supernatants were concentrated with a Retro-X concentrator (Takara). PBMCs were stimulated for 2 days with anti-CD3/anti-CD28 T cell activation beads (Thermo Fisher Scientific, catalog no. 11131D) in the presence of interleukin-2 (IL-2; 40 IU/ml; R&D Systems, catalog no. 202-IL-010) in AIM V media (Thermo Fisher Scientific) supplemented with 5% human serum (Sigma-Aldrich, catalog no. H3667) and incubated at 37°C/5% CO_2. Bead-stimulated cells were transferred to RetroNectin-coated (Takara) virus–containing plates and incubated overnight. Transduction was repeated the next day before counting and diluting cells to 0.4×10^6 cells/ml. After the second transduction, cells were grown for an additional 7 days before removing beads using a DynaMag-15 magnet (Thermo Fisher Scientific). IL-2 was replenished every 2 days to 40 IU/ml. Cells were frozen in 90% fetal calf serum/10% dimethyl sulfoxide and stored in liquid nitrogen.

Trogocytosis assay

CAR T cells were cocultured with target cells at the specified effector-target ratio. Target cells were first labeled with BioTracker 555 (Sigma-Aldrich, catalog no. SCT107) according to the manufacturer's instructions. After the specified amount of time, cells were stained with antibodies and 4′,6-diamidine-2′-phenylindole dihydrochloride (DAPI; 500 ng/ml; Invitrogen, catalog no. D1306). Samples were analyzed on an LSR II flow cytometer (BD).

Flow cytometry–based cytotoxicity assay

A flow cytometry–based cytotoxicity assay was used to determine CAR T cell cytotoxicity against healthy T cells from the same healthy donor and primary MM cells. T cells were isolated from PBMCs using negative selection (STEMCELL Technologies, EasySep Human T Cell Isolation Kit) from autologous healthy donor PBMCs. MM cells and T cells were stained with CellTrace Far Red dye (CTD, Invitrogen) according to the manufacturer's instructions. Target cells at 5×10^4 cells per well were cocultured with different amounts of CAR T cells overnight in a round-bottom 96-well plate at 37°C/5% CO_2. After coculture, Accucheck counting beads (Life Technologies) and DAPI (500 ng/ml) were added to the cells. DAPI⁻CTD⁺ T cells were immediately quantified on an LSR II flow cytometer (BD). To determine killing of T cell subsets and healthy B cells by CD229 CAR T cells, autologous PBMCs were stained with CTD and cocultured with the respective CAR T cells at an effector-target ratio of 2:1 for 6 hours. Subsequently, cocultures were stained with DAPI, and antibodies against CD3, CD4, CD19, CD62L, and CD45RA (table S2) and Accucheck counting beads (Life Technologies) were added to the cells. DAPI⁻CTD⁺ T cells were immediately quantified on an LSR II flow cytometer (BD). Killing of T cell subsets and B cells was determined on a full-spectrum Aurora flow cytometer (Cytek).

Luciferase-based cytotoxicity assay

To determine the cytotoxicity of variant CD229 CAR T cells against the MM cell lines U266B1 and MM.1S, as well as chronic lymphocytic leukemia cell line K562, cell lines were transduced with pHIV-Luc-ZsGreen lentivirus and sorted on a FACSaria flow cytometer (BD) for GFP expression. CD229-negative K562 cells were also transduced with a CD229 expression construct as previously described (19). As with the flow cytometry–based cytotoxicity assay, 5×10^4 target cells were seeded in each well of a round-bottom 96-well plate. Various ratios of CAR T cells were cocultured with target cells overnight at 37°C/5% CO_2. After the coculture, cells were suspended by gentle pipetting, and 100 μl was moved to a 96-well black flat-bottom plate. D-Luciferin at 150 μg/ml (Gold Biotechnology, catalog no. LUCNA-2G) was added to the cells and incubated for 5 min at 37°C. Luminescence was determined on a multimode plate reader (Tecan Spark). For the rechallenge assay, luminescence was determined daily before adding 5×10^4 target cells to each well.

TRF assays

Two different TRF assays were used. To determine the concentration of scFv in the PPEs, 250 ng of rat anti-FLAG (clone L5, BioLegend) in 50 μl of phosphate-buffered saline (PBS) was immobilized on a black 96-well plate (Greiner Bio-One) overnight at 4°C. Plates were washed using an automated plate washer (Tecan HydroFlex) twice with PBS containing 0.1% Tween 20 and twice with PBS in between each incubation. After immobilization, all

other incubations were performed at room temperature at 400 rpm. After immobilization, plates were blocked in 3% nonfat milk in PBS (M-PBS). Then, PPEs or purified 2D3 was added to plates in 3% M-PBS and incubated for 1 hour. Next, plates were incubated with 250 ng of biotinylated protein L (Thermo Fisher Scientific) in 3% M-PBS for 1 hour. Last, plates were incubated with SA-europium (PerkinElmer) in PBS for 30 min. After a final wash, plates were incubated with DELFIA Enhancement solution (PerkinElmer) for 10 min. TRF was determined on a multimode plate reader (Tecan Spark). A purified parental 2D3 standard was used to calculate the scFv concentration in each PPE.

To determine the relative binding of variant scFvs to CD229, recombinant human CD229 (5 µg/ml; R&D Systems) was immobilized on a black 96-well plate (Greiner Bio-One) overnight at 4°C. After immobilization, plates were washed between each step and incubated at room temperature at 400 rpm as described above. Afterward, plates were blocked in 3% M-PBS. Then, plates were incubated with 100 ng of each scFv in 3% M-PBS. Next, plates were incubated with anti-FLAG M2 (Sigma-Aldrich) in 3% M-PBS. Last, plates were incubated with anti-mouse immunoglobulin G (IgG)–europium antibody (PerkinElmer) for 1 hour. After a final wash, plates were incubated with DELFIA Enhancement solution (PerkinElmer) for 10 min. TRF was determined on a multimode plate reader (Tecan Spark).

Biolayer interferometry
SA biosensors (ForteBio) were hydrated in 1× Octet Kinetics Buffer (Sartorius) for at least 10 min before use. SA biosensors were loaded using Octet K2 (Sartorius). A baseline in Octet Kinetics Buffer was collected for 1 min. Then, the sensors were loaded with variant scFvs using a threshold of 2 nm and subsequently blocked in biocytin. Once loaded, sensors were placed back into the sensor tray and kept hydrated in kinetics buffer. Once sensors were loaded, a kinetic run was performed. SA biosensors loaded with 2 nm of biotinylated scFv and blocked with biocytin went through a 60-s baseline read in kinetics buffer, a 50-s association in 2, 1, 0.5, and 0.25 µM recombinant human CD229 (R&D Systems) in kinetics buffer, and, finally, a 60-s dissociation in kinetics buffer. BLI was run at 30°C and 1000 rpm. Data were analyzed using Octet K2 System Data Analysis 9.0 software.

2D3 structure prediction
The structure of the wild-type 2D3 scFv was generated using AlphaFold2 with default parameters (*48*). Structures were visualized using UCSF ChimeraX.

Western blot
Total lysates were extracted from CAR T cells on day 9 of production using radioimmunoprecipitation assay buffer (Thermo Fisher Scientific). Protein concentrations were determined by BCA assay (Thermo Fisher Scientific), samples were separated by SDS–polyacrylamide gel electrophoresis, and separated proteins were transferred to nitrocellulose membranes using an iBlot2 transfer system (Thermo Fisher Scientific). Membranes were blocked with 5% nonfat milk–tris-buffered saline and incubated with primary antibodies against BATF3, pc-Jun (S73), c-Jun, and β-actin (see table S2). Membranes were washed and developed using species-specific secondary anti-IgG/horseradish peroxidase antibodies and Western Lightning Plus-ECL solution (PerkinElmer). Bands were visualized

on an iBright 1500 imaging system (Thermo Fisher Scientific), and bands were quantified using ImageJ software.

MM xenograft mouse model
Six- to 8-week-old male NSG or NRG (the Jackson Laboratory) mice were irradiated with a sublethal dose of 200 to 300 cGy (Rad Source, RS-2000) and injected on the next day through the lateral tail vein with the indicated numbers of U266B1 (NSG) or MM.1S (NRG) cells stably expressing luciferase (Fig. 7, C and D). On day 7 after tumor cell injection, 5×10^6 CD229 CAR T cells or CAR T cells lacking a binding domain (ΔscFv) were injected into the tail vein. To determine in vivo CAR T cell expansion, animals were euthanized 5 days after CAR T cell injection, and spleens were harvested for analysis by flow cytometry. To determine CAR T cell efficacy, animals were weighed twice weekly and monitored for signs of distress in accordance with institutional regulations. For in vivo imaging, mice received an intraperitoneal injection of 3.3 mg of D-luciferin. Photographic and luminescent images were acquired starting 10 min after the D-luciferin injection in both prone and supine positions using an in vivo imaging system (IVIS). Myeloma progression was monitored every 7 days until the study end point. Average radiance (photons per second per square centimeter per steradian) was quantified for individual animals using Living Image software (PerkinElmer).

In vivo cytotoxicity assay using human PBMCs
Eight-week-old male NSG mice were irradiated with a sublethal dose of 300 cGy (Rad Source, RS-2000) and, on the following day, injected with 5×10^6 PBMCs from a healthy human donor. On day 2 after PBMC injection, mice were injected with 5×10^6 CD229 CAR T cells by tail vein. On day 5 after PBMC injection, animals were euthanized, and spleens were collected for flow cytometry analysis. After a 5-min incubation in red blood cell lysis buffer (BioLegend), cells were washed twice in PBS, incubated with human and mouse FcR blocking reagents (Miltenyi Biotec) for 15 min, and then stained with population-specific antibodies (table S2) and DAPI for 30 min. Stained samples were analyzed on an LSR II flow cytometer (BD), and cell numbers were normalized using counting beads (Thermo Fisher Scientific).

CodePlex secretome assay
Supernatants were harvested from overnight cocultures and stored at −80°C until further use. On the day of the assay, samples were thawed, and 11 µl of supernatant per sample was added to CodePlex Human Adaptive Immune secretome chips (Isoplexis). Chips were loaded into the Isolight reader, and cytokines were measured using default settings. Automated analysis of raw data was performed using IsoSpeak (Isoplexis).

Statistical analysis
Significance of differences in cell numbers, CD229 density, and mean fluorescence intensity was calculated by two-sided Student's t test. Significance of differences in T cell and B cell viability after coculture with CD229 CAR T cells was determined by one-way analysis of variance (ANOVA) followed by Tukey's post hoc test. Significance of differences in viability between T cell subsets treated with high- and low-affinity CAR T cells was determined by two-way ANOVA followed by Tukey's post hoc test. Differences in luminescence at individual time points during in vivo

Vander Mause *et al.*, *Sci. Transl. Med.* **15**, eadd7900 (2023)   19 July 2023

14 of 16

experiments were determined by Mann-Whitney *U* test. Statistical significance of differences in survival was determined by log-rank test. All statistical tests were performed using Prism 9 (GraphPad Software). Results were considered significant when *P* or adjusted *P* < 0.05.

Supplementary Materials

This PDF file includes:
Figs. S1 to S13
Tables S1 and S2

Other Supplementary Material for this manuscript includes the following:
MDAR Reproducibility Checklist
Data file S1

View/request a protocol for this paper from *Bio-protocol*.

REFERENCES AND NOTES

1. M. Sadelain, CD19 CAR T cells. *Cell* **171**, 1471 (2017).
2. N. Raje, J. Berdeja, Y. Lin, D. Siegel, S. Jagannath, D. Madduri, M. Liedtke, J. Rosenblatt, M. V. Maus, A. Turka, L.-P. Lam, R. A. Morgan, K. Friedman, M. Massaro, J. Wang, G. Russotti, Z. Yang, T. Campbell, K. Hege, F. Petrocca, M. T. Quigley, N. Munshi, J. N. Kochenderfer, Anti-BCMA CAR T-cell therapy bb2121 in relapsed or refractory multiple myeloma. *N. Engl. J. Med.* **380**, 1726–1737 (2019).
3. A. Mullard, FDA approves 100th monoclonal antibody product. *Nat. Rev. Drug Discov.* **20**, 491–495 (2021).
4. M. A. Cheever, J. P. Allison, A. S. Ferris, O. J. Finn, B. M. Hastings, T. T. Hecht, I. Mellman, S. A. Prindiville, J. L. Viner, L. M. Weiner, L. M. Matrisian, The prioritization of cancer antigens: A national cancer institute pilot project for the acceleration of translational research. *Clin. Cancer Res.* **15**, 5323–5337 (2009).
5. S. Sun, H. Hao, G. Yang, Y. Zhang, Y. Fu, Immunotherapy with CAR-modified T cells: Toxicities and overcoming strategies. *J. Immunol. Res.* **2018**, 2386187 (2018).
6. A. V. Hirayama, C. J. Turtle, Toxicities of CD19 CAR-T cell immunotherapy. *Am. J. Hematol.* **94**, S42–S49 (2019).
7. M. Mamonkin, R. H. Rouce, H. Tashiro, M. K. Brenner, A T-cell-directed chimeric antigen receptor for the selective treatment of T-cell malignancies. *Blood* **126**, 983–992 (2015).
8. X. Liu, N. Zhang, H. Shi, Driving better and safer HER2-specific CARs for cancer therapy. *Oncotarget* **8**, 62730–62741 (2017).
9. R. A. Morgan, J. C. Yang, M. Kitano, M. E. Dudley, C. M. Laurencot, S. A. Rosenberg, Case report of a serious adverse event following the administration of T cells transduced with a chimeric antigen receptor recognizing ERBB2. *Mol. Ther.* **18**, 843–851 (2010).
10. M. Chmielewski, A. Hombach, C. Heuser, G. P. Adams, H. Abken, T cell activation by antibody-like immunoreceptors: Increase in affinity of the single-chain fragment domain above threshold does not increase T cell activation against antigen-positive target cells but decreases selectivity. *J. Immunol.* **173**, 7647–7653 (2004).
11. X. Liu, S. Jiang, C. Fang, S. Yang, D. Olalere, E. C. Pequignot, A. P. Cogdill, N. Li, M. Ramones, B. Granda, L. Zhou, A. Loew, R. M. Young, C. H. June, Y. Zhao, Affinity-tuned ErbB2 or EGFR chimeric antigen receptor T cells exhibit an increased therapeutic index against tumors in mice. *Cancer Res.* **75**, 3596–3607 (2015).
12. F. Turatti, M. Figini, E. Balladore, P. Alberti, P. Casalini, J. D. Marks, S. Canevari, D. Mezzanzanica, Redirected activity of human antitumor chimeric immune receptors is governed by antigen and receptor expression levels and affinity of interaction. *J. Immunother.* **30**, 684–693 (2007).
13. S. Ghorashian, A. M. Kramer, S. Onuoha, G. Wright, J. Bartram, R. Richardson, S. J. Albon, J. Casanovas-Company, F. Castro, B. Popova, K. Villanueva, J. Yeung, W. Vetharoy, A. Guvenel, P. A. Wawrzyniecka, L. Mekkaoui, G. W.-K. Cheung, D. Pinner, J. Chu, G. Lucchini, J. Silva, O. Ciocarlie, A. Lazareva, S. Inglott, K. C. Gilmour, G. Ahsan, M. Ferrari, S. Manzoor, K. Champion, T. Brooks, A. Lopes, A. Hackshaw, F. Farzaneh, R. Chiesa, K. Rao, D. Bonney, S. Samarasinghe, N. Goulden, A. Vora, P. Veys, R. Hough, R. Wynn, M. A. Pule, P. J. Amrolia, Enhanced CAR T cell expansion and prolonged persistence in pediatric patients with ALL treated with a low-affinity CD19 CAR. *Nat. Med.* **25**, 1408–1414 (2019).
14. T. Heitner, A. Moor, J. L. Garrison, C. Marks, T. Hasan, J. D. Marks, Selection of cell binding and internalizing epidermal growth factor receptor antibodies from a phage display library. *J. Immunol. Methods* **248**, 17–30 (2001).

15. J. Yang, S. Baskar, K. Y. Kwong, M. G. Kennedy, A. Wiestner, C. Rader, Therapeutic potential and challenges of targeting receptor tyrosine kinase ROR1 with monoclonal antibodies in B-cell malignancies. *PLOS ONE* **6**, –e21018 (2011).
16. M. Hudecek, M.-T. Lupo-Stanghellini, P. L. Kosasih, D. Sommermeyer, M. C. Jensen, C. Rader, S. R. Riddell, Receptor affinity and extracellular domain modifications affect tumor recognition by ROR1-specific chimeric antigen receptor T cells. *Clin. Cancer Res.* **19**, 3153–3164 (2013).
17. D. Atanackovic, J. Panse, Y. Hildebrandt, A. Jadczak, S. Kobold, Y. Cao, J. Templin, S. Meyer, H. Reinhard, K. Bartels, N. Lajmi, A. R. Zander, A. H. Marx, C. Bokemeyer, N. Kröger, Surface molecule CD229 as a novel target for the diagnosis and treatment of multiple myeloma. *Haematologica* **96**, 1512–1520 (2011).
18. G. Carulli, G. Buda, A. Azzarà, E. M. Ciancia, P. Sammuri, C. Domenichini, V. Guerri, M. Petrini, CD229 expression on bone marrow plasma cells from patients with multiple myeloma and monoclonal gammopathies of uncertain significance. *Acta Haematol.* **135**, 11–14 (2015).
19. S. V. Radhakrishnan, T. Luetkens, S. D. Scherer, P. Davis, E. R. Vander Mause, M. L. Olson, S. Yousef, J. Panse, Y. Abdiche, K. D. Li, R. R. Miles, W. Matsui, A. L. Welm, D. Atanackovic, CD229 CAR T cells eliminate multiple myeloma and tumor propagating cells without fratricide. *Nat. Commun.* **11**, 798 (2020).
20. S. Yousef, M. Kovacsovics-Bankowski, M. E. Salama, N. Bhardwaj, M. Steinbach, A. Langemo, T. Kovacsovics, J. Marvin, M. Binder, J. Panse, N. Kroger, T. Luetkens, D. Atanackovic, CD229 is expressed on the surface of plasma cells carrying an aberrant phenotype and chemotherapy-resistant precursor cells in multiple myeloma. *Hum. Vaccin. Immunother.* **11**, 1606–1611 (2015).
21. M. Hamieh, A. Dobrin, A. Cabriolu, S. J. C. van der Stegen, T. Giavridis, J. Mansilla-Soto, J. Eyquem, Z. Zhao, B. M. Whitlock, M. M. Miele, Z. Li, K. M. Cunanan, M. Huse, R. C. Hendrickson, X. Wang, I. Riviere, M. Sadelain, CAR T cell trogocytosis and cooperative killing regulate tumour antigen escape. *Nature* **568**, 112–116 (2019).
22. M. L. Olson, E. R. V. Mause, S. V. Radhakrishnan, J. D. Brody, A. P. Rapoport, A. L. Welm, D. Atanackovic, T. Luetkens, Low-affinity CAR T cells exhibit reduced trogocytosis, preventing rapid antigen loss, and increasing CAR T cell expansion. *Leukemia* **36**, 1943–1946 (2022).
23. I. C. Nicholson, K. A. Lenton, D. J. Little, T. Decorso, F. T. Lee, A. M. Scott, H. Zola, A. W. Hohmann, Construction and characterisation of a functional CD19 specific single chain Fv fragment for immunotherapy of B lineage leukaemia and lymphoma. *Mol. Immunol.* **34**, 1157–1165 (1997).
24. T. Tiller, I. Schuster, D. Deppe, K. Siegers, R. Strohner, T. Herrmann, M. Berenguer, D. Poujol, J. Stehle, Y. Stark, M. Heßling, D. Daubert, K. Felderer, S. Kaden, J. Kölln, M. Enzelberger, S. Urlinger, A fully synthetic human Fab antibody library based on fixed VH/VL framework pairings with favorable biophysical properties. *MAbs* **5**, 445–470 (2013).
25. S.-J. Wu, J. Luo, K. T. O'Neil, J. Kang, E. R. Lacy, G. Canziani, A. Baker, M. Huang, Q. M. Tang, T. S. Raju, S. A. Jacobs, A. Teplyakov, G. L. Gilliland, Y. Feng, Structure-based engineering of a monoclonal antibody for improved solubility. *Protein Eng. Des. Sel.* **23**, 643–651 (2010).
26. G. A. Weiss, C. K. Watanabe, A. Zhong, A. Goddard, S. S. Sidhu, Rapid mapping of protein functional epitopes by combinatorial alanine scanning. *Proc. Natl. Acad. Sci. U.S.A.* **97**, 8950–8954 (2000).
27. R. L. Petersen, Strategies using bio-layer interferometry biosensor technology for vaccine research and development. *Biosensors (Basel)* **7**, 49 (2017).
28. A. H. Long, W. M. Haso, J. F. Shern, K. M. Wanhainen, M. Murgai, M. Ingaramo, J. P. Smith, A. J. Walker, M. E. Kohler, V. R. Venkateshwara, R. N. Kaplan, G. H. Patterson, T. J. Fry, R. J. Orentas, C. L. Mackall, 4-1BB costimulation ameliorates T cell exhaustion induced by tonic signaling of chimeric antigen receptors. *Nat. Med.* **21**, 581–590 (2015).
29. R. C. Lynn, E. W. Weber, E. Sotillo, D. Gennert, P. Xu, Z. Good, H. Anbunathan, J. Lattin, R. Jones, V. Tieu, S. Nagaraja, J. Granja, C. F. A. de Bourcy, R. Majzner, A. T. Satpathy, S. R. Quake, M. Monje, H. Y. Chang, C. L. Mackall, c-Jun overexpression in CAR T cells induces exhaustion resistance. *Nature* **576**, 293–300 (2019).
30. M. R. Dyson, E. Masters, D. Pazeraitis, R. L. Perera, J. L. Syrjanen, S. Surade, N. Thorsteinson, K. Parthiban, P. C. Jones, M. Sattar, G. Wozniak-Knopp, F. Rueker, R. Leah, J. McCafferty, Beyond affinity: Selection of antibody variants with optimal biophysical properties and reduced immunogenicity from mammalian display libraries. *MAbs* **12**, 1829335 (2020).
31. M. Poorebrahim, J. Melief, Y. P. de Coaña, S. L. Wickström, A. Cid-Arregui, R. Kiessling, Counteracting CAR T cell dysfunction. *Oncogene* **40**, 421–435 (2021).
32. L. Gattinoni, C. A. Klebanoff, D. C. Palmer, C. Wrzesinski, K. Kerstann, Z. Yu, S. E. Finkelstein, M. R. Theoret, S. A. Rosenberg, N. P. Restifo, Acquisition of full effector function in vitro paradoxically impairs the in vivo antitumor efficacy of adoptively transferred CD8+ T cells. *J. Clin. Invest.* **115**, 1616–1626 (2005).
33. J. A. Fraietta, S. F. Lacey, E. J. Orlando, I. Pruteanu-Malinici, M. Gohil, S. Lundh, A. C. Boesteanu, Y. Wang, R. S. O'Connor, W.-T. Hwang, E. Pequignot, D. E. Ambrose, C. Zhang, N. Wilcox, F. Bedoya, C. Dorfmeier, F. Chen, L. Tian, H. Parakandi, M. Gupta, R. M. Young, F. B. Johnson, I. Kulikovskaya, L. Liu, J. Xu, S. H. Kassim, M. M. Davis, B. L. Levine, N. V. Frey, D. L. Siegel, A. C. Huang, E. J. Wherry, H. Bitter, J. L. Brogdon, D. L. Porter,

C. H. June, J. J. Melenhorst, Determinants of response and resistance to CD19 chimeric antigen receptor (CAR) T cell therapy of chronic lymphocytic leukemia. *Nat. Med.* **24**, 563–571 (2018).

34. M. A. de la Fuente, V. Tovar, N. Villamor, N. Zapater, P. Pizcueta, E. Campo, J. Bosch, P. Engel, Molecular characterization and expression of a novel human leukocyte cell-surface marker homologous to mouse Ly-9. *Blood* **97**, 3513–3520 (2001).

35. C. C. Kloss, M. Condomines, M. Cartellieri, M. Bachmann, M. Sadelain, Combinatorial antigen recognition with balanced signaling promotes selective tumor eradication by engineered T cells. *Nat. Biotechnol.* **31**, 71–75 (2013).

36. E. Lanitis, M. Poussin, A. W. Klattenhoff, D. Song, R. Sandaltzopoulos, C. H. June, D. J. Powell Jr., Chimeric antigen receptor T cells with dissociated signaling domains exhibit focused antitumor activity with reduced potential for toxicity in vivo. *Cancer Immunol. Res.* **1**, 43–53 (2013).

37. K. T. Roybal, J. Z. Williams, L. Morsut, L. J. Rupp, I. Kolinko, J. H. Choe, W. J. Walker, K. A. McNally, W. A. Lim, Engineering T cells with customized therapeutic response programs using synthetic notch receptors. *Cell* **167**, 419–432.e16 (2016).

38. A. M. Tousley, M. C. Rotiroti, L. Labanieh, L. W. Rysavy, S. P. Rietberg, E. L. de la Serna, G. N. Dalton, D. Klysz, E. W. Weber, W.-J. Kim, P. Xu, E. Sotillo, A. R. Dunn, C. L. Mackall, R. G. Majzner, Coopting T cell proximal signaling molecules enables Boolean logic-gated CAR T cell control. bioRxiv 2022.06.17.496457 [**Preprint**]. 17 June 2022. https://doi.org/10.1101/2022.06.17.496457.

39. V. D. Fedorov, M. Themeli, M. Sadelain, PD-1- and CTLA-4-based inhibitory chimeric antigen receptors (iCARs) divert off-target immunotherapy responses. *Sci. Transl. Med.* **5**, 215ra172 (2013).

40. S. Arcangeli, M. C. Rotiroti, M. Bardelli, L. Simonelli, C. F. Magnani, A. Biondi, E. Biagi, S. Tettamanti, L. Varani, Balance of anti-CD123 chimeric antigen receptor binding affinity and density for the targeting of acute myeloid leukemia. *Mol. Ther.* **25**, 1933–1945 (2017).

41. C. Roddie, J. Dias, M. A. O'Reilly, M. Abbasian, A. Cadinanos-Garai, K. Vispute, L. Bosshard-Carter, M. Mitsikakou, V. Mehra, H. Roddy, J. A. Hartley, V. Spanswick, H. Lowe, B. Popova, L. Clifton-Hadley, G. Wheeler, J. Olejnik, A. Bloor, D. Irvine, L. Wood, M. A. V. Marzolini, S. Domning, F. Farzaneh, M. W. Lowdell, D. C. Linch, M. A. Pule, K. S. Peggs, Durable responses and low toxicity after fast off-rate CD19 chimeric antigen receptor-T therapy in adults with relapsed or refractory B-cell acute lymphoblastic leukemia. *J. Clin. Oncol.* **39**, 3352–3363 (2021).

42. E. Drent, M. Themeli, R. Poels, R. de Jong-Korlaar, H. Yuan, J. de Bruijn, A. C. M. Martens, S. Zweegman, N. van de Donk, R. W. J. Groen, H. M. Lokhorst, T. Mutis, A rational strategy for reducing on-target off-tumor effects of CD38-chimeric antigen receptors by affinity optimization. *Mol. Ther.* **25**, 1946–1958 (2017).

43. F. Pojero, J. Flores-Montero, L. Sanoja, J. J. Pérez, N. Puig, B. Paiva, S. Bottcher, J. J. van Dongen, A. Orfao; EuroFlow group, Utility of CD54, CD229, and CD319 for the identification of plasma cells in patients with clonal plasma cell diseases. *Cytometry B Clin. Cytom.* **90**, 91–100 (2016).

44. Z. Lin, X. Tang, Y. Cao, L. Yang, M. Jiang, X. Li, J. Min, B. Chen, Y. Yang, C. Gu, CD229 interacts with RASAL3 to activate RAS/ERK pathway in multiple myeloma proliferation. *Aging (Albany NY)* **14**, 9264–9279 (2022).

45. L. Labanieh, R. G. Majzner, D. Klysz, E. Sotillo, C. J. Fisher, J. G. Vilches-Moure, K. Z. B. Pacheco, M. Malipatlolla, P. Xu, J. H. Hui, T. Murty, J. Theruvath, N. Mehta, S. A. Yamada-Hunter, E. W. Weber, S. Heitzeneder, K. R. Parker, A. T. Satpathy, H. Y. Chang, M. Z. Lin, J. R. Cochran, C. L. Mackall, Enhanced safety and efficacy of protease-regulated CAR-T cell receptors. *Cell* **185**, 1745–1763.e22 (2022).

46. H.-S. Li, N. M. Wong, E. Tague, J. T. Ngo, A. S. Khalil, W. W. Wong, High-performance multiplex drug-gated CAR circuits. *Cancer Cell* **40**, 1294–1305.e4 (2022).

47. D. J. Schofield, A. R. Pope, V. Clementel, J. Buckell, S. Chapple, K. F. Clarke, J. S. Conquer, A. M. Crofts, S. R. Crowther, M. R. Dyson, G. Flack, G. J. Griffin, Y. Hooks, W. J. Howat, A. Kolb-Kokocinski, S. Kunze, C. D. Martin, G. L. Maslen, J. N. Mitchell, M. O'Sullivan, R. L. Perera, W. Roake, S. P. Shadbolt, K. J. Vincent, A. Warford, W. E. Wilson, J. Xie, J. L. Young, J. McCafferty, Application of phage display to high throughput antibody generation and characterization. *Genome Biol.* **8**, R254 (2007).

48. J. Jumper, R. Evans, A. Pritzel, T. Green, M. Figurnov, O. Ronneberger, K. Tunyasuvunakool, R. Bates, A. Žídek, A. Potapenko, A. Bridgland, C. Meyer, S. A. A. Kohl, A. J. Ballard, A. Cowie, B. Romera-Paredes, S. Nikolov, R. Jain, J. Adler, T. Back, S. Petersen, D. Reiman, E. Clancy, M. Zielinski, M. Steinegger, M. Pacholska, T. Berghammer, S. Bodenstein, D. Silver, O. Vinyals, A. W. Senior, K. Kavukcuoglu, P. Kohli, D. Hassabis, Highly accurate protein structure prediction with AlphaFold. *Nature* **596**, 583–589 (2021).

Vander Mause *et al.*, *Sci. Transl. Med.* **15**, eadd7900 (2023)   19 July 2023

16 of 16

Science Translational Medicine

Systematic single amino acid affinity tuning of CD229 CAR T cells retains efficacy against multiple myeloma and eliminates on-target off-tumor toxicity

Erica R. Vander Mause, Jillian M. Baker, Kenneth A. Dietze, Sabarinath V. Radhakrishnan, Thierry Iraguha, Destiny Omili, Patricia Davis, Sadie L. Chidester, Katarzyna Modzelewska, Jens Panse, James E. Marvin, Michael L. Olson, Mary Steinbach, David P. Ng, Carol S. Lim, Djordje Atanackovic, and Tim Luetkens

View the article online
https://www.science.org/doi/10.1126/scitranslmed.add7900
Permissions
https://www.science.org/help/reprints-and-permissions

Use of this article is subject to the Terms of service